546370

Prediction of the Extent and Permeability of the Disturbed Rock Zone
around a WIPP Disposal Room
Revision 0

SANDIA NATIONAL LABORATORIES
WASTE ISOLATION PILOT PLANT

Analysis Report for
Prediction of the Extent and Permeability of the Disturbed Rock Zone
around a WIPP Disposal Room

Task 1.4.1.2

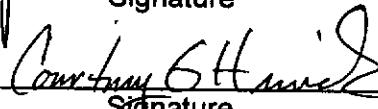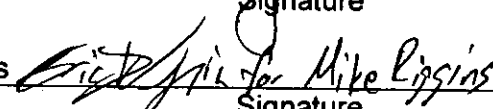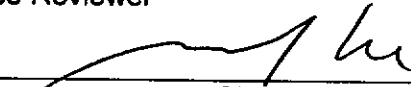|			
Authored by:	Byoung Yoon Park	*(signature)*	6/25/2007
	Print Name	Signature	Date
Authored by:	Ahmed E. Ismail	*(signature)*	6/25/2007
	Print Name	Signature	Date
Authored by:	David J. Holcomb	*(signature)* for David J. Holcomb	6/25/2007
	Print Name	Signature	Date
Authored by:	Courtney G. Herrick	*(signature)*	6/25/07
	Print Name	Signature	Date
Reviewed by:	Michael Riggins	*(signature)* for Mike Riggins	6/25/07
	Print Name	Signature	Date
	Technical Reviewer		
Reviewed by:	Mario J. Chavez	*(signature)*	6/25/07
	Print Name	Signature	Date
	Quality Assurance Reviewer		
Approved by:	Moo Y. Lee	*(signature)*	6/25/07
	Print Name	Signature	Date
	Department Manager		

1.4.1.2: 6/26/07 RH
WIPP:1.4.1:PA:QA-L:545583

Intentionally blank

Acknowledgements

Intentionally Blank

CONTENTS

FIGURES

TABLES

NOMENCLATURE

BRAGFLO	Brine And Gas FLOw (a numerical code)
CCA	Compliance Certification Application
COTS	Commercial Off-The-Shelf
CVS	Concurrent Version System
DPOT	Damage POTential
DRZ	Disturbed Rock Zone
FEM	Finite Element Method
MB	Maker Bed
PA	Performance Assessment
PABC	Performance Assessment Baseline Calculations
PAVT	Performance Assessment Verification Test
PDB	Parameter Data Base
QA	Quality Assurance
SS	Simplified Stratigraphy
WIPP	Waste Isolation Pilot Plant
WTS	Washington TRU Solutions

1 INTRODUCTION

1.1 Background

The Waste Isolation Pilot Plant (WIPP) repository is excavated in a halite layer of the Salado Formation, just above one of the thicker anhydrite layers known as Marker Bed (MB) 139. The stress state is sufficient to promote considerable creep deformation of halite. In addition, fracturing is commonly observed near the excavation surfaces. Compared to other rocks, salt creeps readily in response to differential stresses. Stress-field alteration and creep closure will create a disturbed rock zone (DRZ) around the excavation. Relative to the intact salt, the DRZ exhibits increased porosity as a result of microfracturing and increased permeability as a result of connecting fractures. Over time, the DRZ properties change as salt creep occurs.

The DRZ is an important feature that is included in the performance assessment (PA) process models to predict future repository conditions and brine flow to the accessible environment. Furthermore, as modeled, the properties of the DRZ control a significant portion of the brine that can flow into the waste rooms. The three fundamental parameters of the DRZ used in the PA analysis are its extent, its porosity, and its permeability.

The DRZ dimensions and permeability ranges used for the performance assessment verification test (PAVT) were not changed for the recent recertification performance assessment baseline calculations (PABC) [Leigh et al. 2005]. However, field measurements, laboratory observations, numerical modeling, and operational experience show that the extent, porosity, and permeability of the DRZ can now be more accurately represented. These properties change with time; in particular, the extent of DRZ decreases as the salt undergoes deformation. In conjunction with this decrease in the extent of the DRZ, its permeability also decreases, thereby limiting the amount of brine that could flow from the Salado Formation into the disposal rooms.

It is clear that the DRZ will be limited in extent over the regulatory period. Hansen [2003] presents the several avenues of scientific approach that lead to this conclusion. Extensive laboratory salt creep data demonstrate that damage can be assessed in terms of volumetric strain and principal stresses. Stress states that cause dilation are defined in terms of stress invariants, which allow reasonable models of DRZ evolution and devolution [Park and Holland, 2004; Park and Holland, 2006]. Permeability measurements performed on WIPP salt show increased permeability with increasing volumetric strain due to creep damage [Stormont, 1990; Pfeifle et al., 1998]. In this analysis report, a procedure to calculate the extent and permeability of the DRZ around a disposal room and the results based on the AP-133 [Park and Ismail, 2007] will be provided. The results of this analysis will be used in BRAGFLO, which simulates the brine and gas flow in and around the repository.

1.2 Objectives

Currently, the DRZ surrounding the WIPP repository is represented by two materials in WIPP PA: DRZ_0, which characterizes the state of the DRZ before closure of the WIPP facility; and DRZ_1, which characterizes the state of the DRZ after closure of the WIPP facility Although it is known that the properties of the DRZ change with time as the salt creeps and interacts with the waste stack and gas pressures from waste decomposition due to degradation, there is currently no material present in the parameter database that takes these changes into account.

The objectives of this report are:

(1) to determine the maximum extent of DRZ above and below the room;

(2) to determine the time at which the dilatancy criterion for the salt surrounding a room is continually satisfied;

(3) to determine the properties of a new material, to be called DRZ_2, which will better reflect the long-term physical properties of halite of the DRZ after satisfaction of the dilatancy criterion.

The information of the extent will be used in composing the BRAGFLO grid. The DRZ_2 material will be used in BRAGFLO to represent the DRZ beyond a certain time to be specified, at which point the dilatancy criterion predicts no damage to the surrounding salt. The method for calculating the properties of DRZ_2 which are not copied directly from either DRZ_0 or DRZ_1 will be outlined below.

1.3   Report Organization

The remainder of this report describes implementation details. Section 2 describes how to calculate the DRZ extent and the permeability distribution around a disposal room. The activity flow diagram of the approach is shown in this section. The procedure to obtain field data for the DRZ depth is briefly mentioned.

Section 3 describes the approach to determine the stratigraphy at Location 1 in S-90 access drift to Room Q for the structural analysis. The constitutive models for halite, argillaceous halite, and anhydrite are presented including the material property data. The mesh and boundary conditions for the FEM analysis show in this section. This section also provides the damage potential contours around the drift and the value of C in the dilatant damage criterion obtained by comparing the analysis result and the field data. Using the revised C value, the DRZ extents around a disposal room at specific times are predicted.

Section 4 illustrates the permeability distribution around a disposal room. The properties of new material parameter DRZ_2, which will be used in BRAGFLO analysis, are provided in this section. Section 5 lists the computer codes used in this analysis and the file naming convention for the calculation. Section 0 provides some additional perspective on these calculations and some concluding remarks. References are provided in Section 7.

2 APPROACH

2.1 Overview

The work outlined in this report follows closely the analysis of the structural response analysis associated with raising the level of disposal rooms from their original position to the level of Clay Seam G [Park, 2002; Park and Holland 2004; Park and Holland, 2006]. The change of DRZ extent with time will be calculated based on a dilatant damage potential criterion. The constant C in the dilatancy criterion will be determined by comparing the numerical analysis results of the Room Q access drift (Location 1 in S-90 drift as shown Figure 1 analysis with the field data obtained by Holcomb and Hardy [2001]. The relationship between the permeability and the volumetric strain of the halite will be defined from the results of a literature survey, while the permeability distribution within the DRZ will be calculated by post-processing the result from Clay Seam G analysis. Figure 2 illustrates the flow diagram for how these calculations feed into determining the DRZ with permeability around a disposal room.

2.2 Extent of the DRZ

The primary task involved in predicting the extent of the DRZ will be a study of the stress responses at Location 1 in the south rib (wall) of the S-90 drift (Location 1) as a function of time. The methods employed will be the same as those used in the Clay Seam G numerical analysis [Park and Holland, 2004; Park and Holland, 2006] in conjunction with ultrasonic wave velocity field results.

Because the geometry of Location 1 differs from that of a disposal room as used in the Clay Seam G analysis, it will be necessary to create a new finite element method (FEM) mesh for use in SANTOS [Stone, 1997b]. SANTOS is a quasistatic, large-deformation finite element code that was used in the Clay Seam G analysis. The stratigraphy at Location 1 will be constructed from the underground geologic log map in Location 1 [Powers, 2000], the stratigraphy near Room Q [Domski et al., 1996], and the idealized stratigraphy of Munson et al. [1989]. The dimensions of the access drift will be determined from the S-90 drift as-built survey [WTS, 1994].

Dilatancy, defined as an increase in volumetric strain under compressive stress [Jaeger and Cook, 1979], is attributed to micro-fracturing or changes in the pore structure of the salt, resulting in an increase in permeability. A dilatant damage criterion is used to delineate potential zones of DRZ in the salt formation. In this analysis, the following dilatancy criterion is used:

$$D = \frac{C \cdot I_1}{\sqrt{J_2}} \quad \dots\dots\dots\dots\dots\dots\dots\dots\dots\dots\dots\dots\dots\dots\dots\dots\dots\dots\dots\dots\dots\dots\dots\dots\dots\dots\dots(1)$$

where D is the damage factor;
C is a constant;
$I_1 = \sigma_1 + \sigma_2 + \sigma_3 = 3\sigma_m$ is the first invariant of the stress tensor;
$J_2 = \dfrac{(\sigma_1 - \sigma_2)^2 + (\sigma_2 - \sigma_3)^2 + (\sigma_3 - \sigma_1)^2}{6}$ is the second invariant of the deviatoric stress tensor;
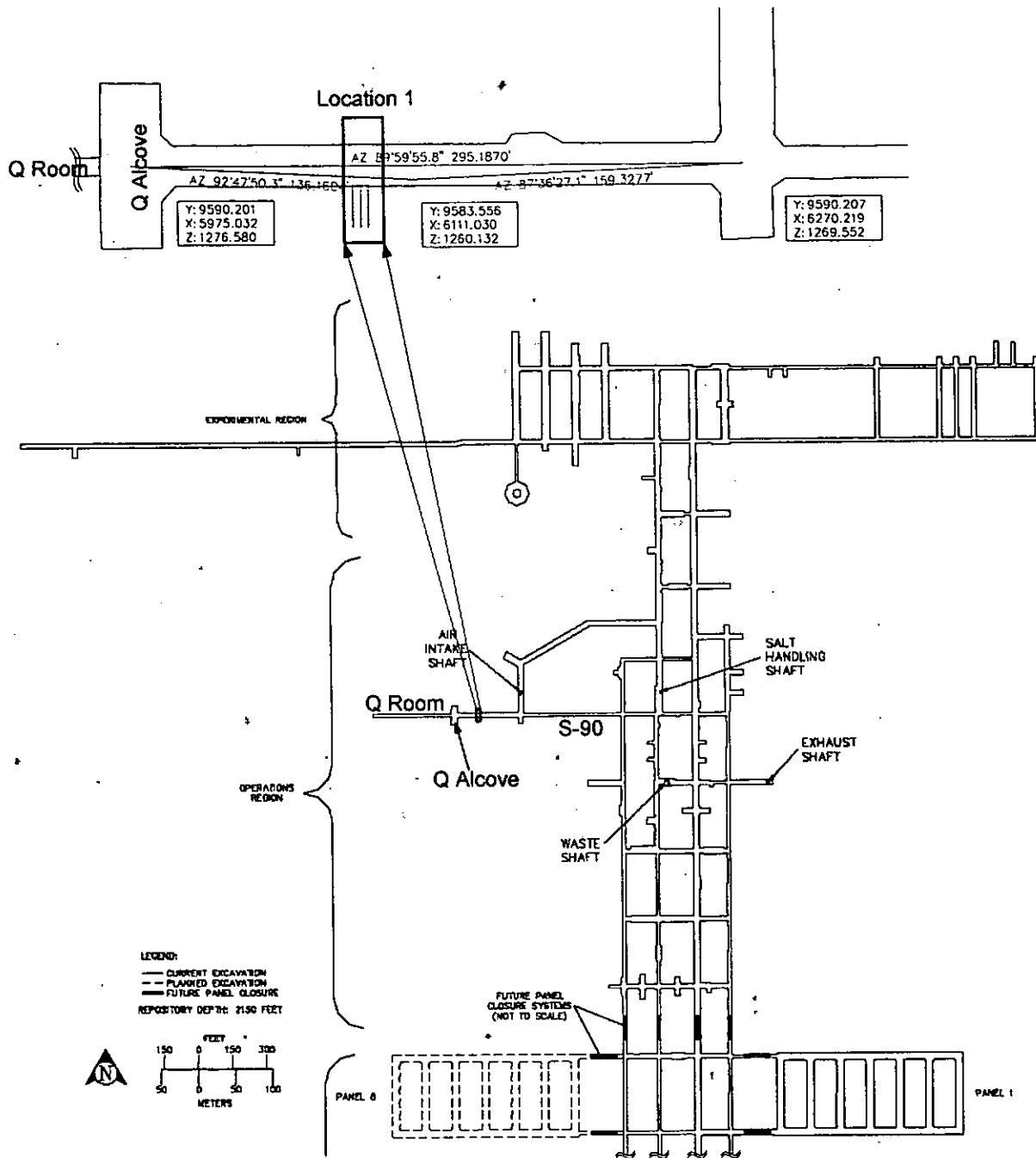
Figure 1: Location 1 in S-90 Drift

QA for Ultrasonic Wave Velocity Test Data

Structural Analysis for Room Q Access Drift using SANTOS

Define the Relationship between Permeability and Volumetric Strain

Draw the Contours for Dilatant Damage Potential
$$D = \frac{C \cdot I_1}{\sqrt{J_2}}$$

Ultrasonic Wave Velocity Test Data

Postprocess Clay Seam G Output using Peach Model
$$k_p = C_p \cdot \varepsilon_V^3$$

Determine the Constant C in the Dilatancy Criterion by Comparing the Contours with Ultrasonic Wave Velocity Test Data

Draw Permeability Distribution around Room based on Strain Distribution from Clay Seam G Analysis

Draw DRZ Extent around Room based on Stress Distribution from Clay Seam G Analysis

Permeability within the DRZ at Specific Times

- Maximum Extent of DRZ
- Time at which DPOT satisfied
- Properties of DRZ_2

BRAGFLO Analyses for Salado

Figure 2: Activity flow diagram for determining the extent and permeability of the DRZ around a WIPP disposal room.

σ_1, σ_2, and σ_3 are the maximum, intermediate, and minimum principal stresses, respectively; and σ_m is the mean stress.

When $D < 1$, the shear stresses in the salt are large relative to the mean stresses, and dilatancy is predicted; similarly, when $D \geq 1$, the shear stresses are small relative to the mean stress, and dilatancy is not predicted.

As mentioned above, the stresses in the DRZ are expected to change as a function of time. Because of salt creep, the dimensions of the Room Q access drift began to decrease as soon as excavation was completed. Thus, knowledge of the amount of time that lapsed between completion of the excavation and the acquisition of the ultrasonic velocity data is necessary to correctly estimate the value of the constant C in the damage criterion (Equation 1).

Using the results obtained from SANTOS, the two stress invariants I_1 and J_2 will be used to plot the contours corresponding to different values of C around the drift. The locations at which the ultrasonic velocity data indicates that there is no salt damage as a result of excavation will be superimposed on the contour plots to determine the value of C. Given the revised value of C, the extent of the DRZ will be assessed by determining the damage factor contours obtained from the Clay Seam G analysis [Park and Holland, 2004; Park and Holland, 2006].

2.3 Ultrasonic Wave Velocity Test Data

Holcomb and Hardy [2001] performed ultrasonic wave speed measurements to characterize the DRZ in Location 1 (Figure 1). Measurements were taken at 30 cm (1 ft) intervals over paths vertical, horizontal, and perpendicular to the drift axis, giving a complete and redundant data set. Measurements were taken using paths through the salt near the back, floor, and center rib to detect how the varying stress state affects the development of the DRZ in these locations. Figure 3 shows the arrangement and naming scheme for the measurement holes in Location 1.

Ultrasonic wave velocities are decreased by open cracks and loosened grain boundaries. The effect is strongest for cracks oriented perpendicular to the particle motion induced by the wave. Thus the physical extent of the disturbed zone can be determined by propagating ultrasonic waves through successive portions of the formation. Cracking responsible for the disturbed zone is expected to vary as a function of distance from the face of rib and to depend on the position of the measurement path relative to the back and floor. The undisturbed zone is defined as that region where the elastic wave speed remains constant with increasing depth from the rib. Measurements were made between pairs of holes ("cross-hole") cored perpendicular to the axis of the drift along horizontal and vertical paths lying in vertical planes parallel to the rib. Between each pair of holes, travel time measurements were made at 30 cm (1 ft) intervals to a depth of about 7 meters (~20 ft), as measured from the rib face. In addition, measurements were made within one hole ("same-hole") along paths perpendicular to the drift wall. The paths for the cross-hole measurements were nominally one meter long, while the same-hole measurements all had the a fixed path length of nominally 33 cm. Travel time measurements were made using the technique commonly used for laboratory determinations of ultrasonic sound velocity in rock, a sound pulse is applied to the rock at a known time and place and, after traveling through the rock, is received by a transducer at a known distance. P- (compression) wave velocity, V_P, and S- (shear) wave velocity, V_S, data will be used for the measurements. The travel time and distance combine to give the average velocity over the path. Figure 4 shows cross-hole P-wave velocity versus the depth from the rib as an example.

Q ACCESS DRIFT BOREHOLE IDENTIFICATION
LOCATION #1

TERRY MACDONALD & WES DEYONGE

SANDIA NATIONAL LABORATORIES, DEPT. 6821

DRZ CHAR. TEST PLAN

03/15/00

BACK

(ARGILLACEOUS)

QGD10 QGD11   QGU10   QGU11   QGU12

(HALITE)

QGD12 QGD13   QGU13   QGU14   QGU15

(MARKER BED)

(ARGILLACEOUS)

QGD14 QGD15   QGU16   QGU17   QGU18

FLOOR

BOREHOLE IDENTIFICATION NUMBER:
Q G D 1 0
          └── BOREHOLE NUMBER
        └───── BOREHOLE SUITE LOCATION (1 & 2 = Q ACCESS DRIFT; 3 & 4 = Q ALCOVE)
      └─────── SPECIFIC TEST (D = DENSITY / MOISTURE; U = ULTRASONIC / ACOUSTIC)
    └───────── TYPE OF TEST (G = GEOPHYSICAL)
  └─────────── ROOM LOCATION (Q = Q ROOM / Q ACCESS DRIFT / Q ALCOVE)

Figure 3: Arrangement and naming scheme for the measurement holes [Holcomb and Hardy, 2001].
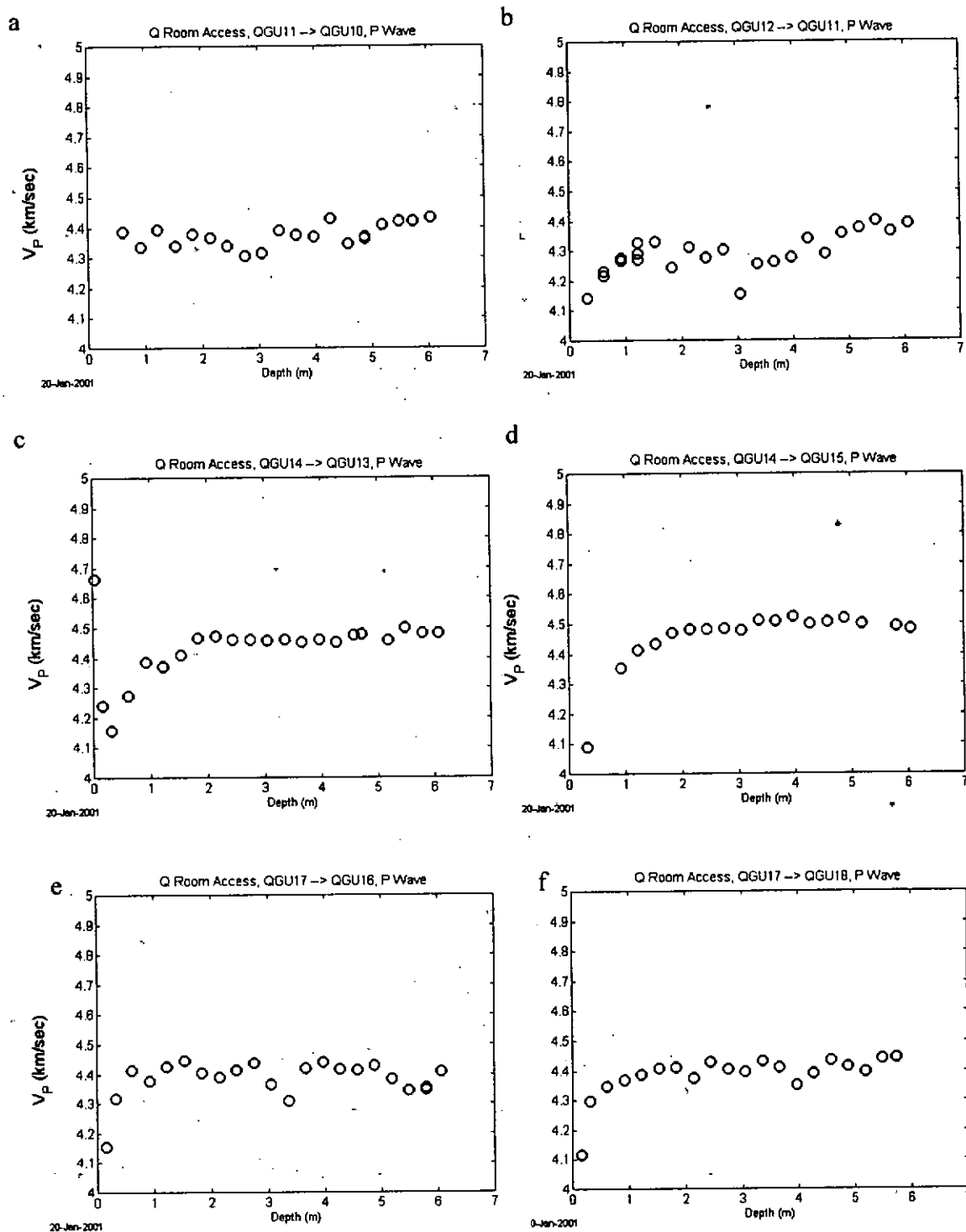
Figure 4. P-wave velocities (V_p) for all horizontal cross-hole paths arranged in the same order as the physical arrangement of holes in the rib [Holcomb and Hardy, 2001].

2.4 Permeability of the DRZ

Within the new DRZ, it is necessary to define a new relationship for the permeability as a function of time. Chan and co-workers [Chan et al., 2001] created a model relating permeability both to strain and to networked porosity. The Chan model is a combination of the Carman-Kozeny model of porosity-based permeability [Carman, 1937] and the theoretical work of Peach on the permeability of damaged salt [Peach, 1991]. Peach uses percolation theory arguments to define the dilatant strain ε as

$$\varepsilon = \frac{2\pi \langle c \rangle^2 \langle w \rangle \alpha}{\langle l \rangle^3} \quad \text{...(2)}$$

where $\langle c \rangle$ is the mean crack radius, $\langle w \rangle$ is the mean crack half-width, α is a volumetric shape factor, and $\langle l \rangle$ is the mean crack spacing. The overall expression for the permeability is given by

$$k = \frac{2}{15} \langle w \rangle^2 \varepsilon \alpha p^* \quad \text{...(3)}$$

where p^* is the fraction of cracks that are part of a connected network. Using the linear relationship between dilatant strain ε and mean crack half-width $\langle w \rangle$, the relationship between permeability and strain can be written as

$$k = \frac{p^* \langle l \rangle^6}{30\pi^2 \alpha \langle c \rangle^4} \varepsilon^3 \quad \text{...(4)}$$

Rather than attempting to evaluate the prefactor in the above expression, Chan et al. [2001] treat the prefactor as a fitting parameter A to be estimated using experimental data, so that the permeability can be written as

$$k = A\varepsilon^3 \quad \text{...(5)}$$

Chan et al. [2001] do not report the details used to obtain their fitting parameter A. Consequently, we will use the data obtained by Pfeifle et al. [1998] to compute a value for the fitting parameter. With this new parameter value, it will be possible to estimate the permeability in the DRZ as a function of time by using strain values calculated using data from the Clay Seam G analysis [Park and Holland, 2004; Park and Holland, 2006]. In particular, the long-term "steady-state" value of the permeability will be used to define a distribution for the parameters DRZ_2:PRMX_LOG, DRZ_2:PRMY_LOG, and DRZ_2:PRMZ_LOG.

2.5 Properties of DRZ_2

In addition to the permeability parameters discussed in the previous section, it will also be necessary to specify the other parameters for DRZ_2. The basic set of parameters which will need to be specified are summarized in Table 1 below.

Most of the property values for DRZ_2 will be taken directly from the corresponding properties of either DRZ_0 or DRZ_1; the exceptions to this are the permeability parameters PRMX_LOG, PRMY_LOG, and PRMZ_LOG, which will be obtained as described above.

Table 1: Basic properties of DRZ_2 to be specified [Definitions listed are from the WIPP PA PDB].

Property	Definition
CAP_MOD	Model number, capillary pressure model
COMP_RCK	Bulk compressibility
KPT	Flag for permeability determined threshold
PC_MAX	Maximum capillary pressure
PCT_A	Threshold pressure constant parameter
PCT_EXP	Threshold pressure exponential parameter
PO_MIN	Minimum brine pressure
PORE_DIS	Pore distribution parameter
POROSITY	Porosity
PRMX_LOG	Log of permeability in the x-direction
PRMY_LOG	Log of permeability in the y-direction
PRMZ_LOG	Log of permeability in the z-direction
RELP_MOD	Relative permeability model number
SAT_IBRN	Initial brine saturation
SAT_RBRN	Residual brine saturation
SAT_RGAS	Residual gas saturation

2.6 DRZ and Permeability around a Disposal Room

The structural analyses for a disposal room were performed to estimate whether raising the repository to Clay Seam G would have any significant impact on the integrity of the repository [Park and Holland, 2004; Park and Holland, 2006]. The calculations used in the Compliance Certification Application (CCA) were replicated and then repeated for a changed grid reflecting the repository being raised to Clay Seam G. The results of the analyses for the current room will be used for calculating the DRZ extent and the permeability around a disposal rooms.

To calculate the DRZ extent at specific times, the stress results will be post-processed using Equation (1), with the value of C determined from the ultrasonic wave velocity measurements. The strain results will be post-processed using Equation (5) to determine the permeability around the disposal room at specific times. The post-processing code ALGEBRA will be used. The permeability distribution around the disposal room will be overlapped with the revised maximum extent of the DRZ. Characteristics of the DRZ at specific times will be provided to the BRAGFLO analyst to modify the grid for DRZ extent and parameters values related to the permeability.

3 STRUCTURAL ANALYSIS AT LOCATION 1 IN S-90 DRIFT

3.1 Determination of Stratigraphy

The ultrasonic wave velocity data was obtained at Location 1 in the south rib (wall) of the S-90 drift that provides access to Room Q. Location 1 is centered near E6085 as shown Figure 5 [Holcomb and Hardy, 2001]. The drift was mined at approximately 655 m. Stratigraphic data at Location 1 is not available. Domski's [1996] stratigraphic map from the Room Q alcove (Figure 6) is the nearest one to Location 1. The elevation of Clay Seam G (Anhydrite "b") was calculated to be approximately 391 m from the scale of y-axis as shown in Figure 6.

Figure 7 shows the idealized stratigraphy defined by Munson et al. [1989] for the two-dimensional structural analysis of WIPP. This contains a number of stratigraphic details, including material layers, material types, and clay seams. Munson et al. [1989] assumed that argillaceous material dominates the stratigraphy beyond the range of the direct observations and core taken from the Room D horizon. The materials are the clean salt, argillaceous salt, anhydrite, and polyhalite.

A narrow vertical graphic profile (Figure 8) was created along S-90 at approximately Location 1 [Powers, 2000]. The elevations of the back and floor of the drift at E6085 are 387.86 m (1272.5 ft) and 384.14 m (1260.3 ft) respectively. Thus the height of the drift is 3.72 m (12.2 ft). The width of the drift is 5.64 m (18.5 ft) [MacDonald, 2000].

A simplified stratigraphy for the drift modeling at Location 1 is modified from Munson et al. (1989) and is shown in Figure 9. The elevation of Clay G, which is the reference elevation (0.00 m in Figure 7, is adjusted to match its elevation of 391 m in Figure 6. Then, the elevations of other clay seams are determined from the reference elevation.
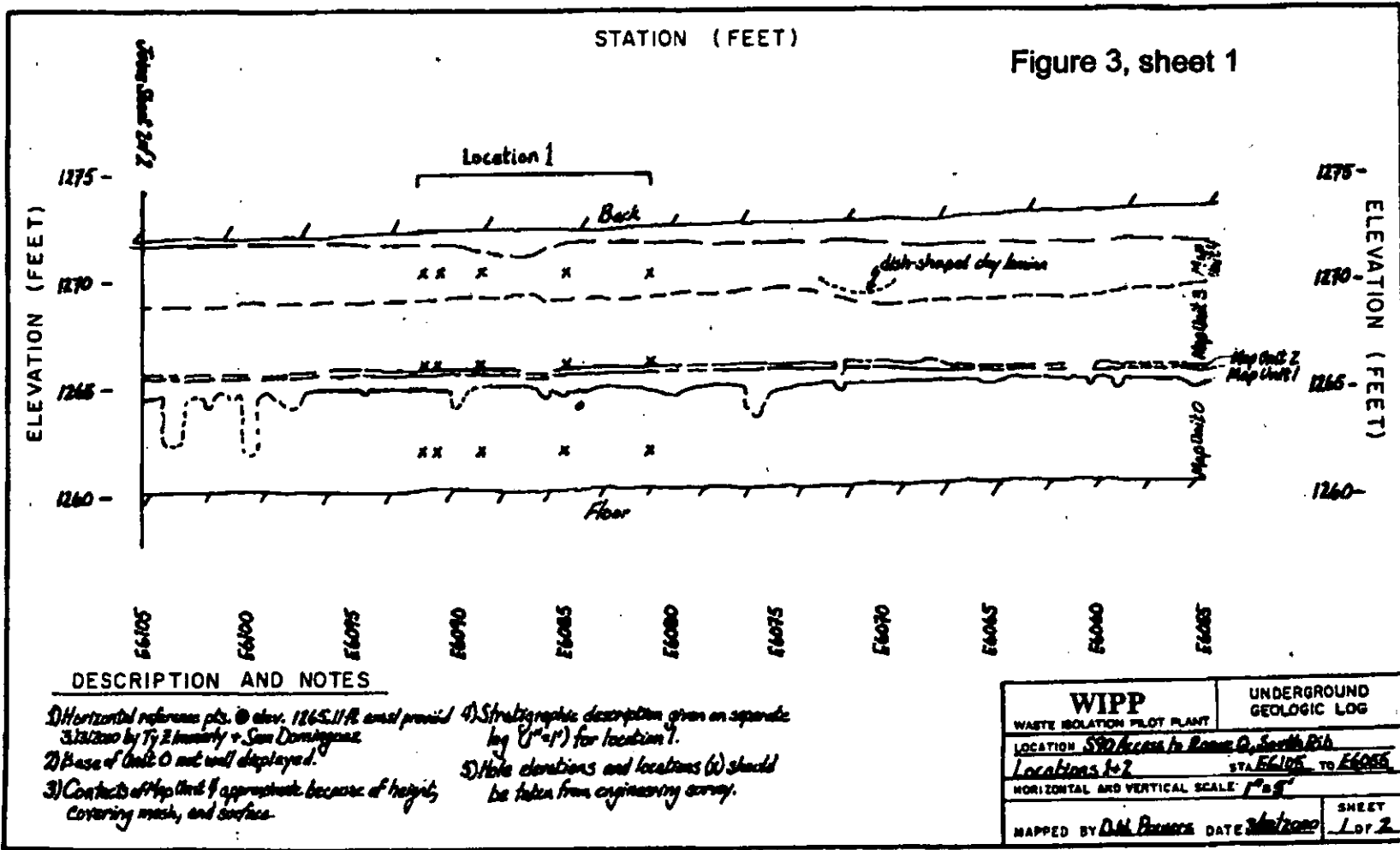
Figure 5: Underground geologic log at S-90 access drift to Room Q, South rib from E6105 to E6055 [Powers, 2000].
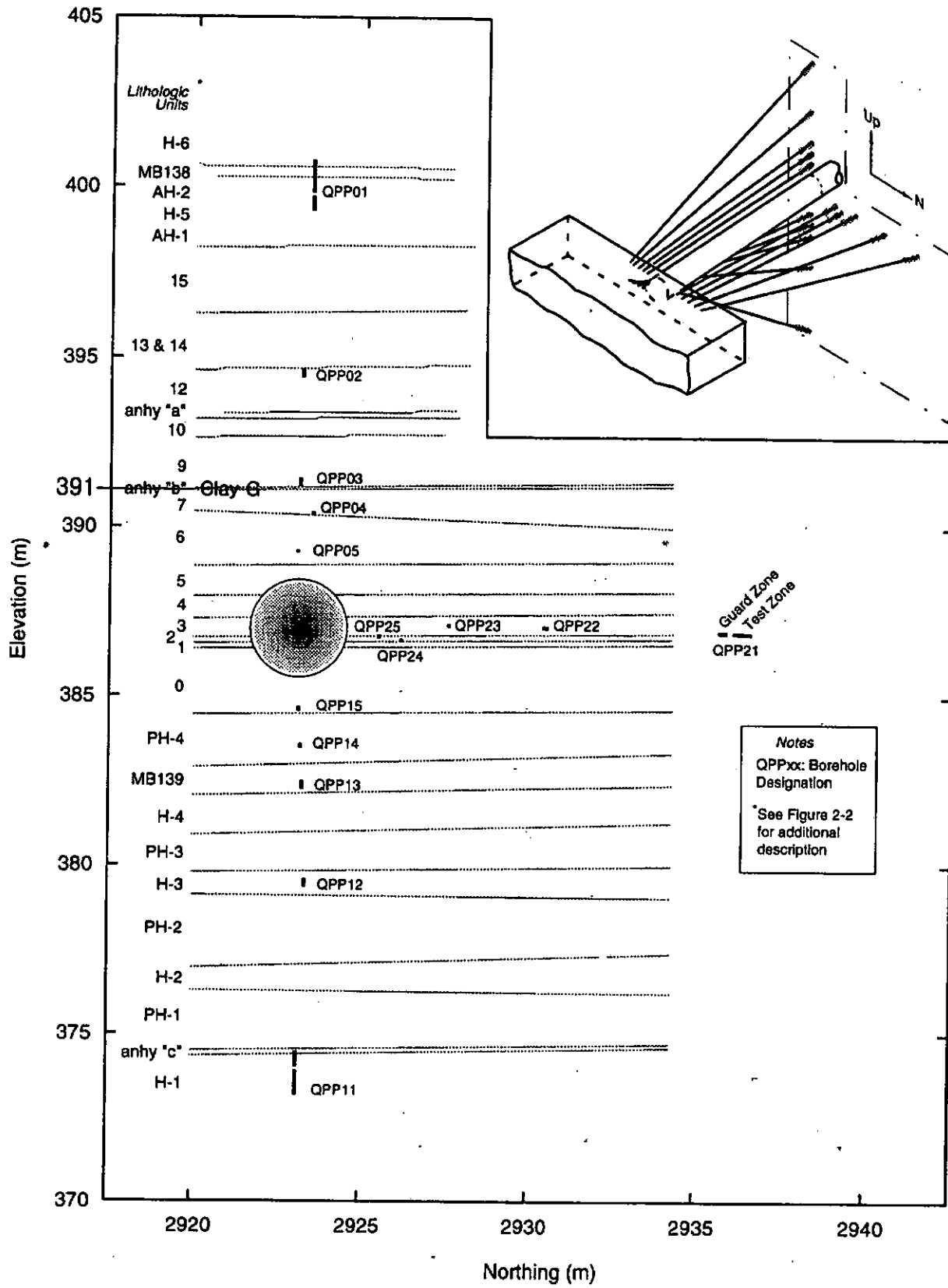
Figure 6: Stratigraphy near the Room Q alcove [Domski, 1996] and the elevation of Clay Seam G.

TRI-6119-233-2
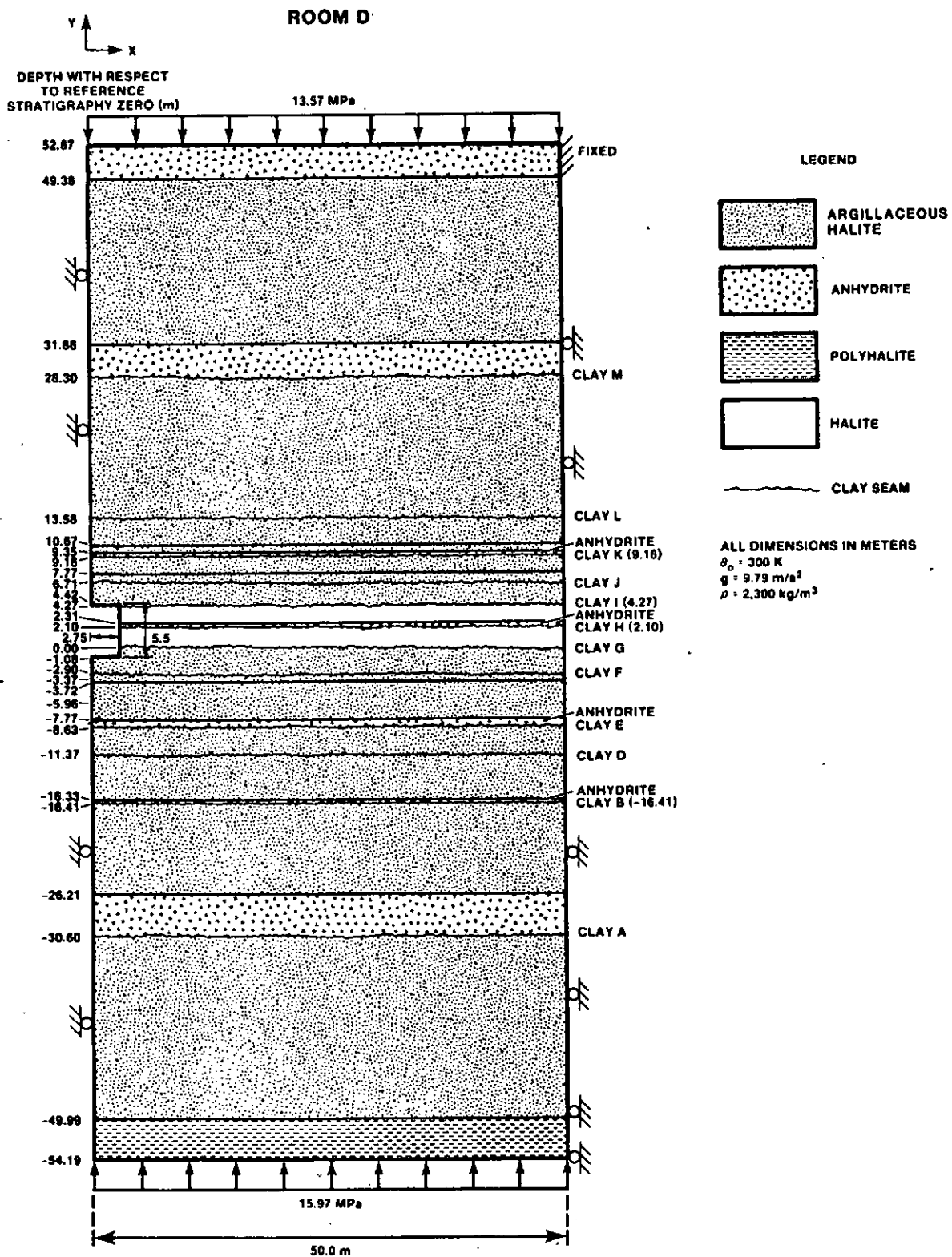
Figure 7: Idealized stratigraphy around Room D [Munson et al., 1989].
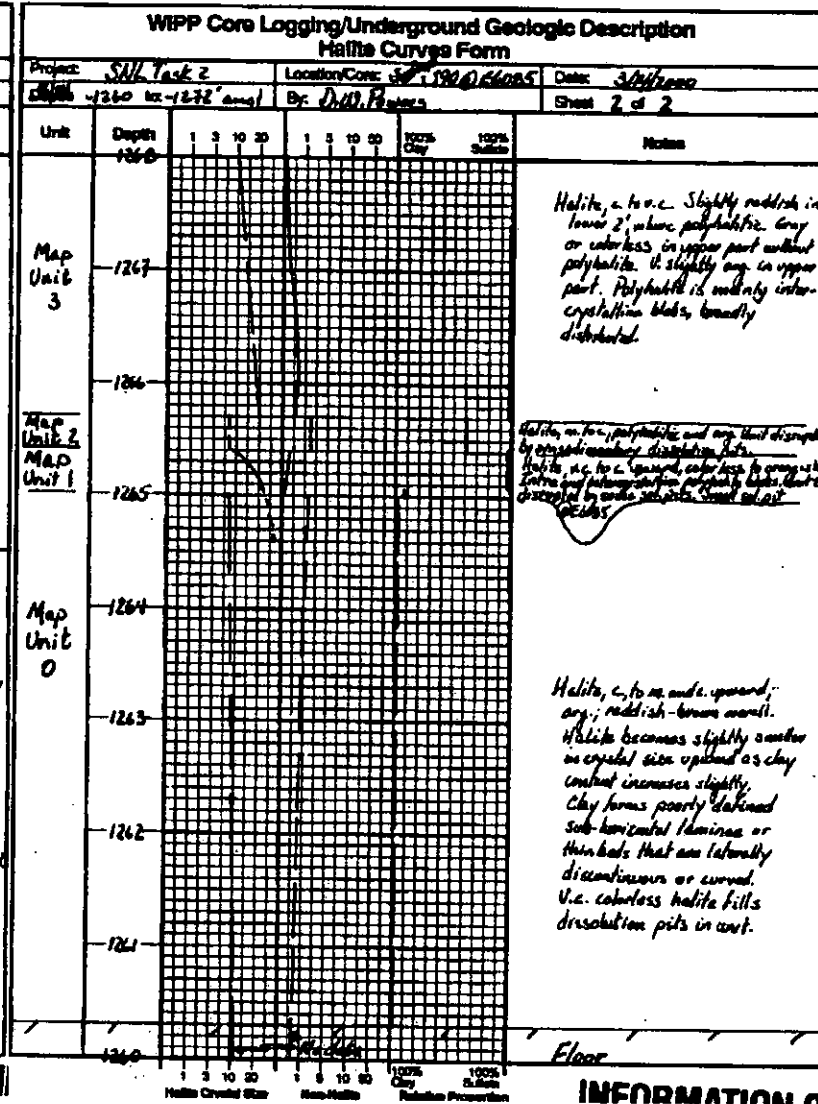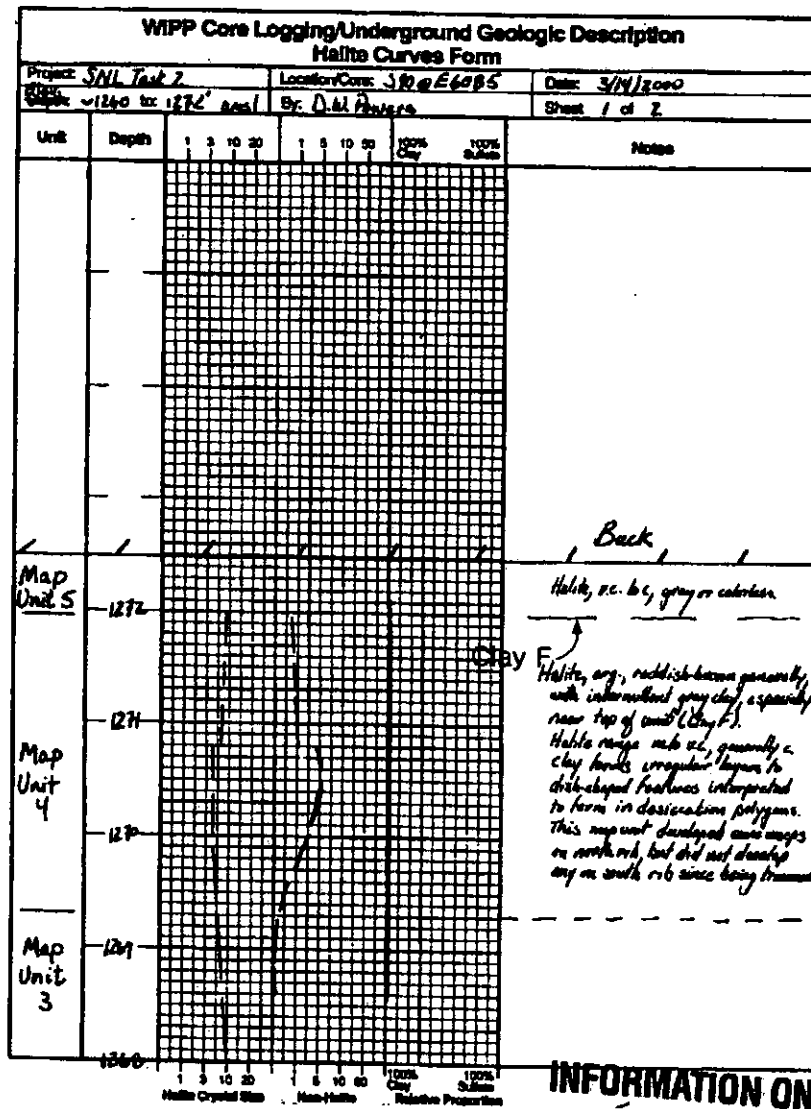
Figure 8: A narrow vertical graphic profile created along S90 at approximately E6085 based on the south rib [Powers, 2000].
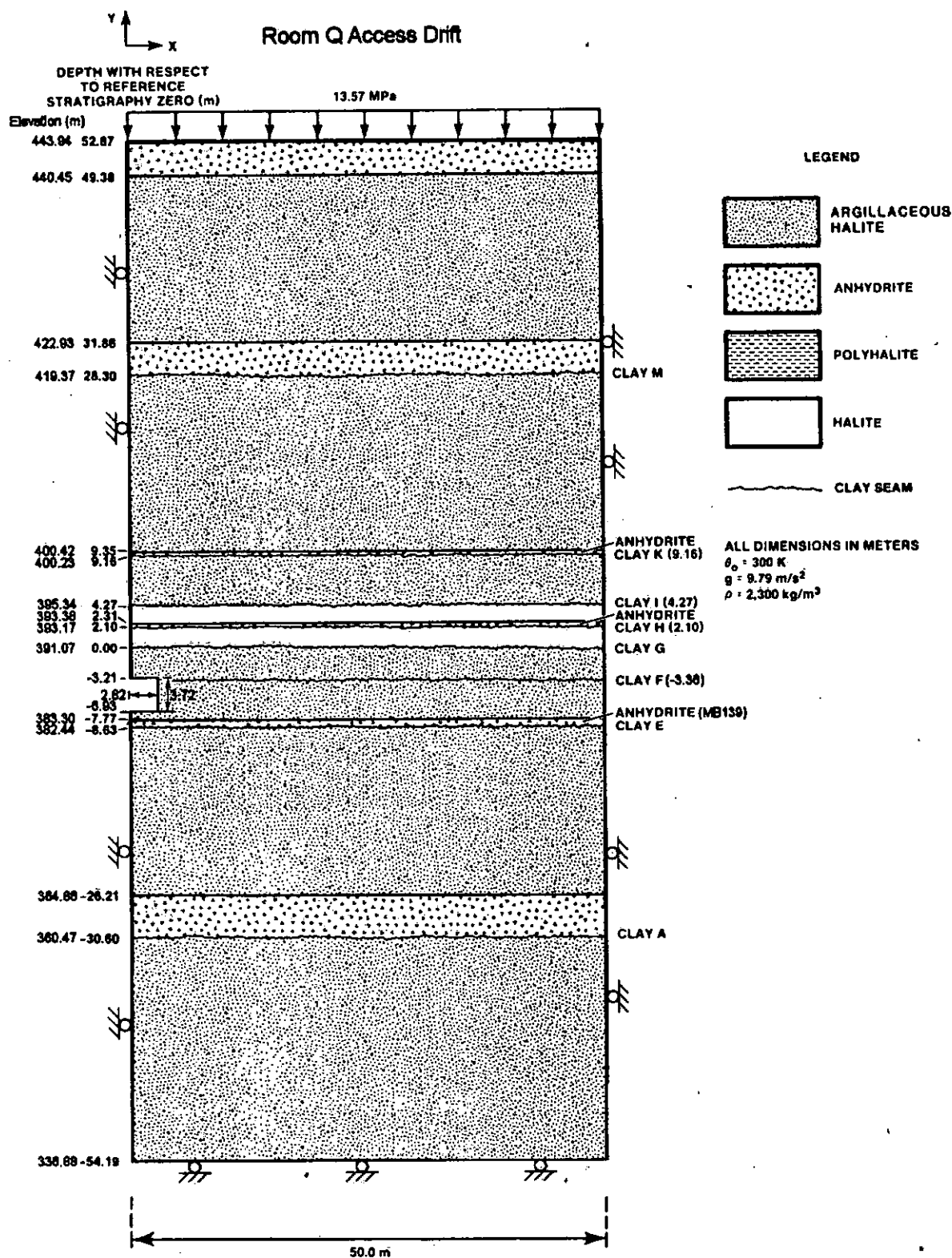
Figure 9: Simplified stratigraphy for Room Q access drift.

3.2 Geomechanical Models

3.2.1 Halite constitutive models

The multi-mechanism deformation (M-D) model proposed by Munson and Dawson [1979; 1982; 1984] and extended by Munson et al. [1989], has been included in SANTOS to model the creep behavior of rock salt. The model can be decomposed into an elastic volumetric part Eq. (6) defined by

$$\varepsilon_{kk} = \frac{\sigma_{kk}}{3K} \quad \text{...(6)}$$

where, ε_{kk} = Total strain components

σ_{kk} = Total stress components

K = Elastic bulk modulus

and a deviatoric part Eq. (7) defined by

$$\dot{s}_{ij} = 2G\left(\dot{e}_{ij} - F\dot{\varepsilon}_s\left[\frac{\cos 2\theta}{\sqrt{J_2}\cos 3\theta}s_{ij} + \frac{\sqrt{3}\sin\theta}{J_2\cos 3\theta}\left\{s_{ip}s_{pj} - \frac{2J_2}{3}\delta_{ij}\right\}\right]\right) \quad \text{.........................(7)}$$

where, $s_{ij} = \sigma_{ij} - \dfrac{\sigma_{kk}}{3}$: Deviatoric stress tensor

G = Elastic shear modulus

$e_{ij} = \varepsilon_{ij} - \dfrac{\varepsilon_{kk}}{3}$: Deviatoric strain tensor

δ_{ij} = Kronecker delta

= 1 for i = j

= 0 for i ≠ j

J_2 and θ are the second invariant of the deviator stress and the Lode angle, respectively.

The second term of Eq. (7) represents the creep contribution. In this creep term of, F, is a multiplier on the steady-state creep rate to simulate the transient creep response according to the following equation,

$$F = \begin{cases} e^{\Delta[1-\zeta/\varepsilon_t^*]^2}, & \zeta < \varepsilon_t^* \\ 1 & \zeta = \varepsilon_t^* \\ e^{-\delta[1-\zeta/\varepsilon_t^*]^2} & \zeta > \varepsilon_t^* \end{cases} \quad \text{...(8)}$$

where, Δ = Work-hardening parameter

δ = Recovery parameter

ε_t^* = Transient strain limit

Finally, ζ is an internal state variable whose rate of change is determined by the following evolutionary equation,

$$\dot{\zeta} = (F-1)\dot{\varepsilon}_s \dotfill (9)$$

In Eq. (8), the work-hardening parameter Δ is defined as,

$$\Delta = \alpha + \beta \log(\bar{\sigma}/G) \dotfill (10)$$

where, α and β are constants. The variable $\bar{\sigma}$ is the equivalent Tresca stress given by

$$\bar{\sigma} = 2\sqrt{J_2} \cos\theta \dotfill (11)$$

where, $\theta = \dfrac{1}{3}\arcsin\left[\dfrac{-3\sqrt{3}J_3}{2(J_2)^{3/2}}\right]$ is the Lode angle limited to the range: $(-\dfrac{\pi}{6} \leq \theta \leq \dfrac{\pi}{6})$.

$J_2 = \dfrac{1}{2}s_{pq}s_{qp}$: second invariant of the stress deviator.

$J_3 = \dfrac{1}{3}s_{pq}s_{qr}s_{rp}$: third invariant of the stress deviator

The recovery parameter, δ, is held constant. The transient strain limit is given by

$$\varepsilon_t^* = K_0 e^{cT}(\bar{\sigma}/G)^M \dotfill (12)$$

where K_0, c, and M are constants.

The steady-state, or secondary creep strain rate, $\dot{\varepsilon}_s$, is given by

$$\dot{\varepsilon}_s = A_1 e^{-Q_1/RT}\left(\frac{\bar{\sigma}}{G}\right)^{n_1} + A_2 e^{-Q_2/RT}\left(\frac{\bar{\sigma}}{G}\right)^{n_2} + |H|\left[B_1 e^{-Q_1/RT} + B_2 e^{-Q_2/RT}\right]\sinh\left[\frac{q(\bar{\sigma}-\sigma_0)}{G}\right] \dotfill (13)$$

where,

A_i's and B_i's = Secondary creep constants

Q_i's = Activation energies

T = Absolute temperature

R = Universal gas constant

n_i's = Stress exponents

q = Stress constant

σ_0 = Stress limit of the dislocation slip mechanism

$|H|$ = Heaviside step function with the argument $(\bar{\sigma} - \sigma_0)$

The material constants corresponding to the clean and argillaceous salt, used in this analysis, are given in Table 2.

Table 2: Material properties of salt used in the analysis

	Parameters		Units	Clean Salt	Argillaceous Salt
Elastic Properties [Butcher, 1997]	Shear modulus	G	MPa	12,400	
	Young's modulus	E	MPa	31,000	
	Poisson's ratio	ν	-	0.25	
Salt Creep Properties [Munson et al., 1989]	Secondary creep constant	A_1	s^{-1}	8.386×10^{22}	1.407×10^{23}
		B_1		6.086×10^6	8.998×10^6
		A_2		9.672×10^{12}	1.314×10^{13}
		B_2		3.034×10^{-2}	4.289×10^{-2}
	Activation energies	Q_1	cal/mole	25,000	25,000
		Q_2	cal/mole	10,000	10,000
	Stress exponents	n_1	-	5.5	5.5
		n_2		5.0	5.0
	Stress limit of the dislocation slip mechanism	$\sigma_{0_{\square}}$	MPa	20.57	20.57
	Stress constant	q	-	5,335	5,335
	Transient strain limit constants	M	-	3.0	3.0
		K_0	-	6.275×10^5	2.470×10^6
		c	K^{-1}	9.198×10^{-3}	9.198×10^{-3}
	Constants for work-hardening parameter	α	-	-17.37	-14.96
		β	-	-7.738	-7.738
	Recovery parameter	δ	-	0.58	0.58

3.2.2 Anhydrite constitutive model

The anhydrite layers both above and below the disposal room are expected to experience inelastic material behavior. The anhydrite layers are assumed to be isotropic and elastic until yield occurs [Butcher, 1997]. Yield is assumed to be governed by the Drucker-Prager (D-P) criterion.

$$\sqrt{J_2} = C - aI_1 \dots\dots(14)$$

where J_2 = the second deviatoric stress invariant (see Equation 1)

I_1 = the first stress invariant (see Equation 1)

A non-associative flow rule is used to determine the plastic strain components. To use the soils and foams model [Stone, 1997b] for the anhydrite layers, SANTOS input parameters were derived from the elastic properties and D-P constants, C and a as given in Table 3. The D-P model is embodied in the soils and foams model in SANTOS.

The input to the soils and foams model in the SANTOS code requires the analyst to provide the shear modulus, μ, and the bulk modulus, K. The conversion from Young's modulus, E, and

Poisson's ratio, v, to the SANTOS input parameters is given by the following relationships taken from Jaeger and Cook [1979]:

$$2\mu = \frac{E}{(1+v)} \quad\text{...(15)}$$

$$K = \frac{E}{3(1-2v)} \quad\text{...(16)}$$

SANTOS requires the input to the material model which describes the anhydrite nonlinear response to be given in terms of effective stress, $\bar{\sigma} = \sqrt{3J_2}$, and pressure, $p = \frac{I_1}{3}$. Rewriting Eq. (14) in terms of $\bar{\sigma}$ and p, the following relationship is obtained:

$$\bar{\sigma} = \sqrt{3}C - 3\sqrt{3}ap \quad\text{...(17)}$$

The SANTOS input constant A_0 is $\sqrt{3}C$ and the input constant A_1 is $3\sqrt{3}a$. The set of SANTOS input parameters for the anhydrite is given in Table 3.

Table 3: Material properties of anhydrite used in the analysis [Butcher, 1997]

Material Property		Units	Anhydrite
Young's modulus		MPa	75,100
Density		kg/m^3	2,300
Poisson's ratio			0.35
Drucker-Prager constants	C	MPa	1.35
	a	-	0.45
Bulk modulus		MPa	83,440
Two mu		MPa	55,630
SANTOS input constants	A$_0$	MPa	2.338
	A$_1$		2.338

3.3 Mesh Generation

A two-dimensional plane-strain drift model is used to represent the drift and surrounding rock (Figure 9). The model grid Figure 10 represents the cross-section of the drift in two dimensions. Invoking symmetry, only half of the drift is modeled. The drift is modeled as being subjected to regional far-field boundary condition acting from an infinite distance away. The distance to the confining boundary is 50 m. This distance is about ten times the width of drift. This ratio is far better than the generally accepted ratio of five for the maximum dimensions to minimum excavation sizes in numerical analysis [Goodman, 1989]. The upper and lower boundaries are located approximately 50 m from the drift. A lithostatic stress ($\sigma_x = \sigma_y = \sigma_z$) that varies with depth is used as the initial stress boundary conditions; gravity forces are included.

A zero-displacement boundary condition in the horizontal direction ($U_X = 0.0$) was applied on both the left and right boundaries of the model to represent the symmetrical nature of a drift and

far-field stresses respectively. A prescribed normal traction of 13.57 MPa was applied on the upper boundary and a vertical zero-displacement boundary condition ($U_Y = 0.0$) was applied on the lower boundary to react to the overburden load. The initial half-symmetry drift dimensions are 3.72 m high by 2.82 m wide. The FASTQ input file used for the mesh generation is provided in Appendix A.
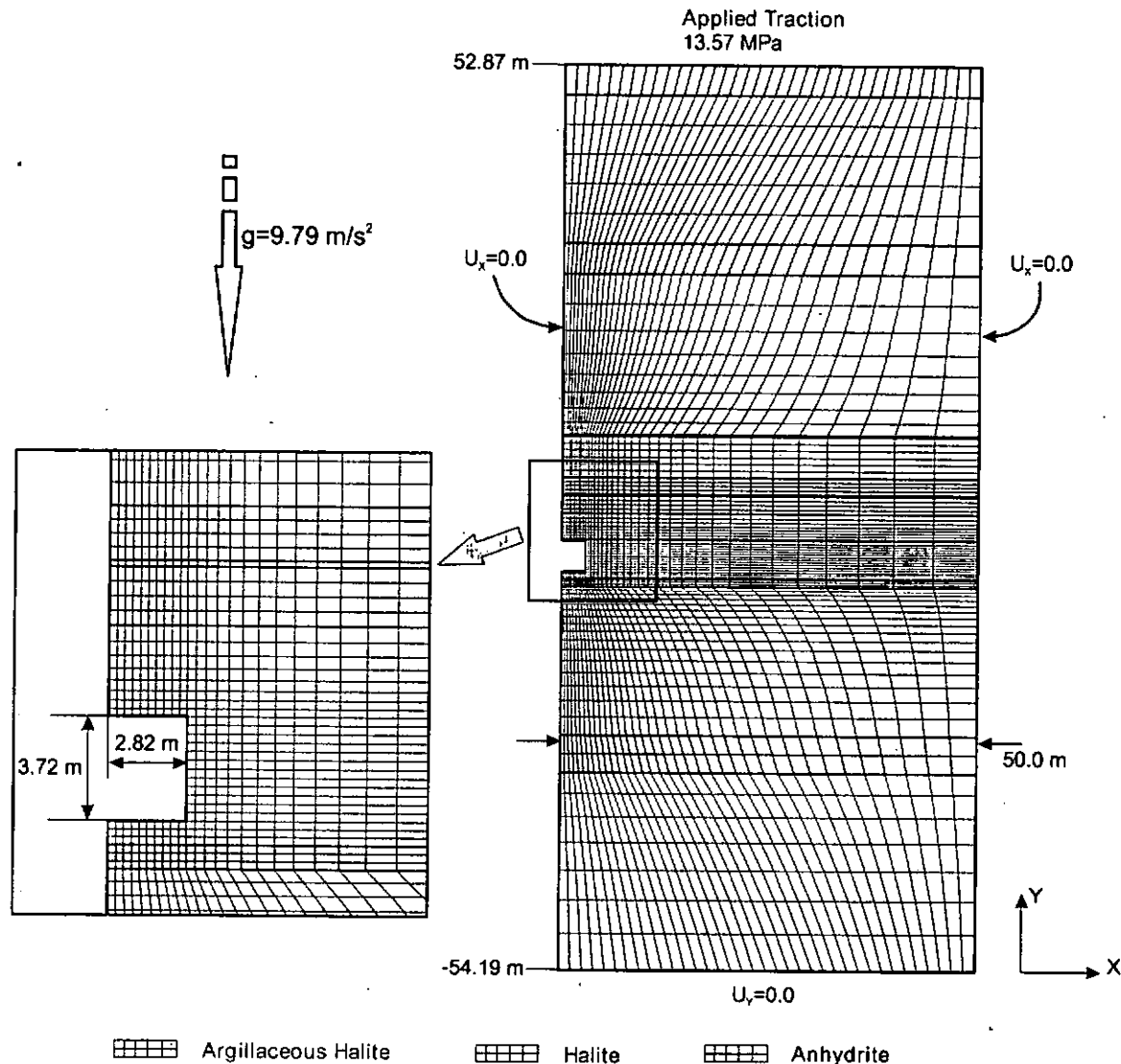
Figure 10: Mesh discretization and boundary conditions around the drift

3.4 Solver

To determine the constant, C, in the dilatancy criterion (see Equation 1), a structural analysis for the Room Q access drift is conducted using the quasistatic, large-deformation finite element code SANTOS [Stone, 1997b]. SANTOS is capable of representing 2D planar or axisymmetric geometries. The solution strategy used to obtain the equilibrium states is based on a self-adaptive, dynamic-relaxation solution scheme incorporating proportional damping. The explicit nature of the code means that no stiffness matrix is formed or factorized, thereby reducing the

amount of computer storage necessary for execution. The element used in SANTOS is a uniform-strain, 4-node, quadrilateral element with an hourglass control scheme to minimize the effects of spurious deformation modes. Constitutive models for many common engineering materials are available within the code. A robust master-slave contact surfaces algorithm for modeling arbitrary sliding contact is implemented. The executable SANTOS version 2.1.7 was installed and qualified on Warthog, a Linux workstation (WIPP PA, 2003). The SANTOS input file for the drift analysis is provided in Appendix B-1. The calculation sheet to compute the SANTOS input parameters using Table 2 and Table 3 is provided in Appendix B-2.

3.5 Damage Potential around the Drift.

The completion date of mining the S- 90 drift from W-620 to Room Q alcove was January 1988. Holcomb and Hardy performed ultrasonic wave speed measurement from May 23 to 25, 2000 and again in August 28 to 29, 2001. Thus the data was acquired at approximately 12.3 years and 13.7 years after excavation of the drift. Salt creep into the drift was accounted for in the FEM modeling.

From the structural analysis for the drift, the dilatancy damage potential (DPOT) around the drift was calculated using Equation (1). Figure 11 show the DPOT contours at 12.3 years and 13.7 years after excavation from the analysis. The DPOT contours correspondent to different C values in Equation (1). A smaller value of constant C in the equation yields a greater extent of damage. To calculate the damage potential in the salt, the post-processing codes ALGEBRA and BLOT are used on the SANTOS Exodus output file to determine the spatial contours of the dilatant damage. The ALGEBRA and BLOT scripts are provided in Appendix C.
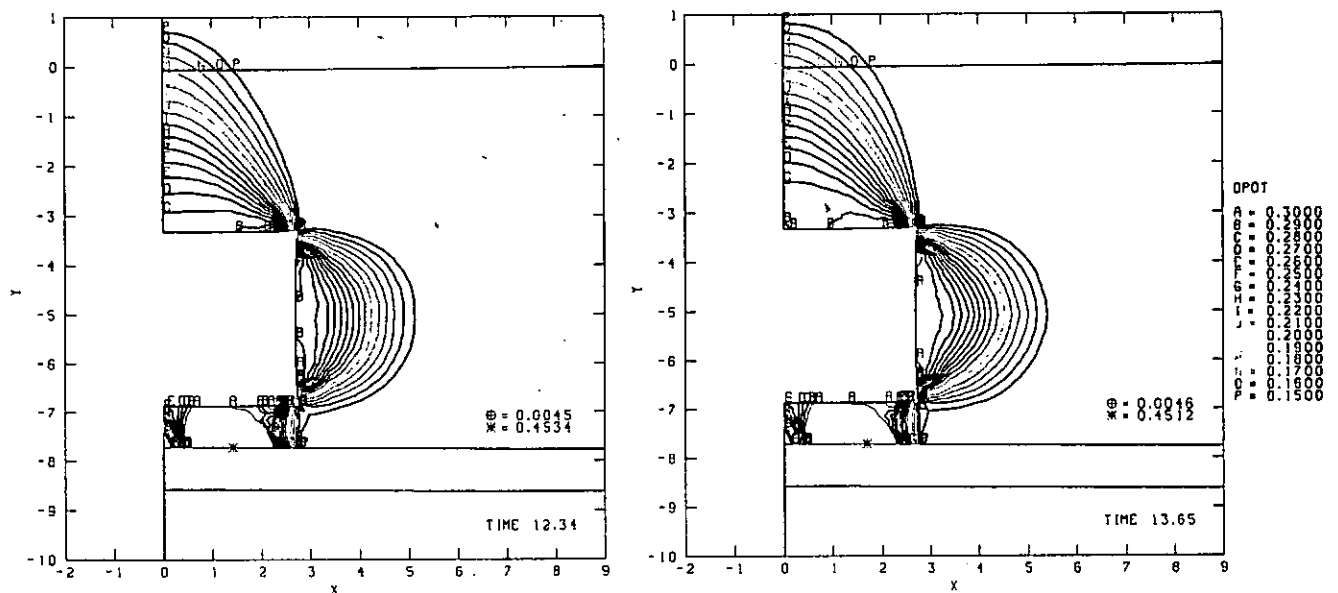
Figure 11: Damage potential contours around the drift at 12.3 years and 13.7 years after the drift excavation (X- and Y- axes in m).

3.6 Inferred DRZ Depth

The depths of DRZ are inferred from the ultrasonic wave velocity data measured as described in Section 2.3. Figure 12 shows the velocity data versus depth as determined on May 25, 2000 from cross-hole P-wave measurements between boreholes QGU14 (Transmitter) and QGU15 (Receiver). The velocity increases from 3.84 km/s at 0.15 m depth to 4.61 km/s at 1.83 m depth. The velocity does not increase beyond 1.9 m depth but exhibits variations around a value of 4.63 km/s. Figure 13 shows the velocity versus depth for a same-hole test in QGU14 using S-waves on August 29, 2001. The velocity increases from 1.04 km/s at 0.15 m depth to 2.73 km/s to 1.83 m depth. No systematic velocity variations were observed beyond 1.8 m, although there were variations about the best-fit value of 2.75 km/s.

A bilinear model was used to describe the velocity-vs.-depth data. To develop the model parameters, a depth was chosen by inspection that marked the deepest extent of the DRZ. Then a line of the form $y=V_0$ was fit to the data points at depths greater than the deepest point of the DRZ and a line of the form $y=ax+b$ was fit to the data points at shallower depths. The fits were done using the trend line capability of MS Excel. V_0, the average velocity beyond the DRZ, is considered to be the wave velocity in the undisturbed salt. The intersection of the trend line $y=ax+b$ and the average value line can be regarded as an inferred DRZ depth. The inferred DRZ depths for Figure 12 and Figure 13 are calculated as 1.719 m and 1.796 m, respectively.

All figures for inferring DRZ depth around the drift are provided in Appendix D.
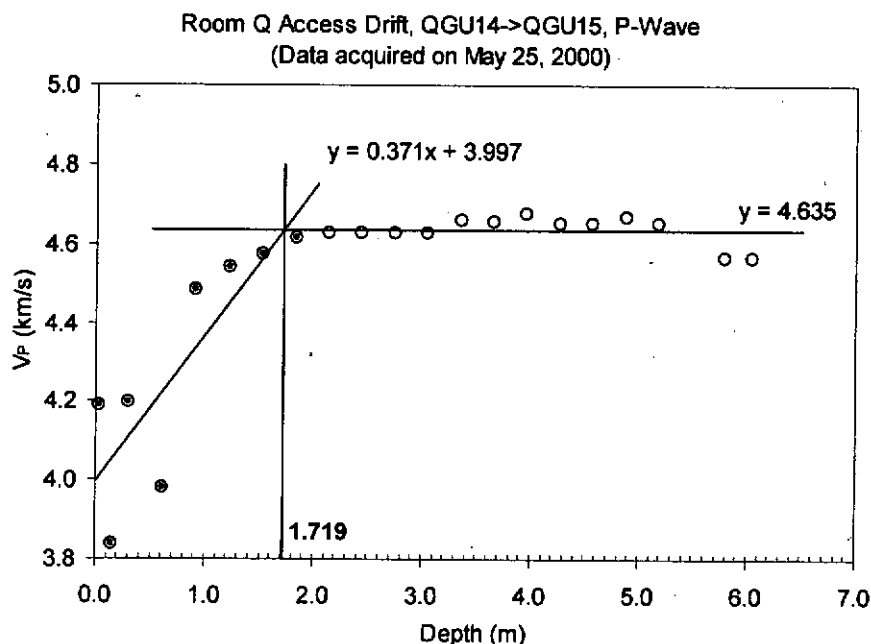
Figure 12: Velocity data versus depth with trend and average lines from a cross-hole test between boreholes QGU14 (Transmitter) and QGU15 (Receiver) using P-wave.

Room Q Access Drift, QGU14->QGU14, S-Wave
(Data acquired on Aug. 29, 2001)
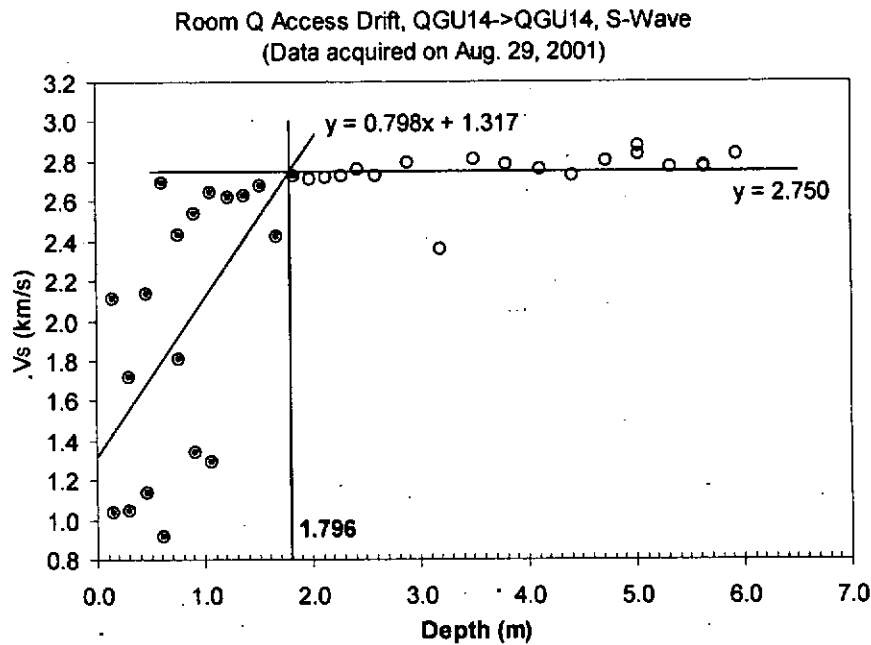
Figure 13: Velocity data versus depth with trend and average lines from a same-hole test in borehole QGU14 using S-wave.

3.7 Determination of C in the Dilatant Damage Criterion

The constant, C, in the dilatant damage criterion (see Equation 1) is determined from the damage potential contours (Figure 11) and the inferred DRZ depth (Appendix D). Figure 14 and Figure 15 show the DPOT contours from the structural analysis of the S-90 drift at Location 1 at 12.34 and 13.67 years respectively after the drift excavation was completed. Inferred DRZ depths as calculated in Appendix D are also plotted on the figures. The constant C is determined from reading the contour values of DPOT corresponding to the DRZ depth data points.
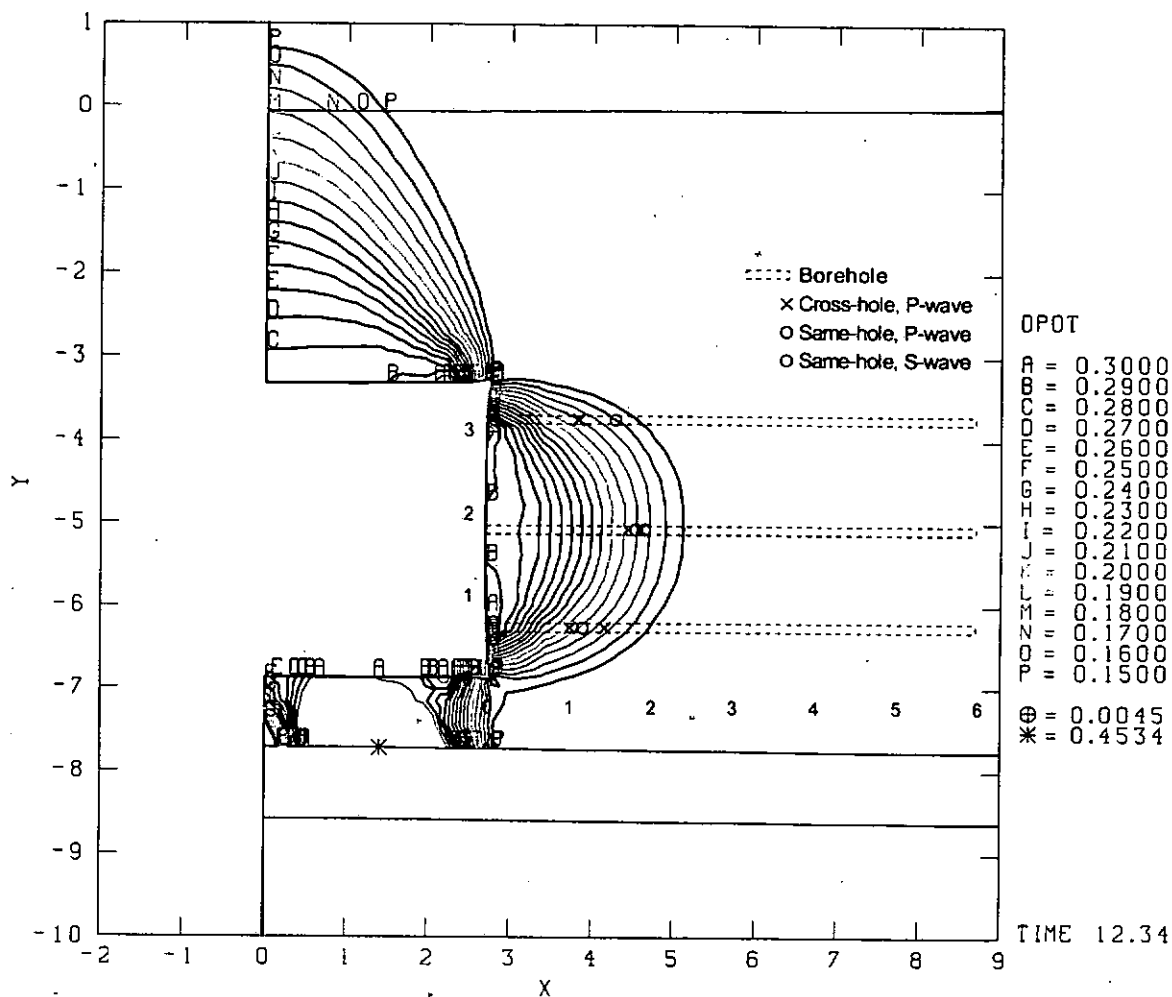
Figure 14: Damage potential contours around S-90 drift at Location 1 including ultrasonic velocity data points, which infer DRZ extent, acquired during May 2000 (X- and Y-axes in m).
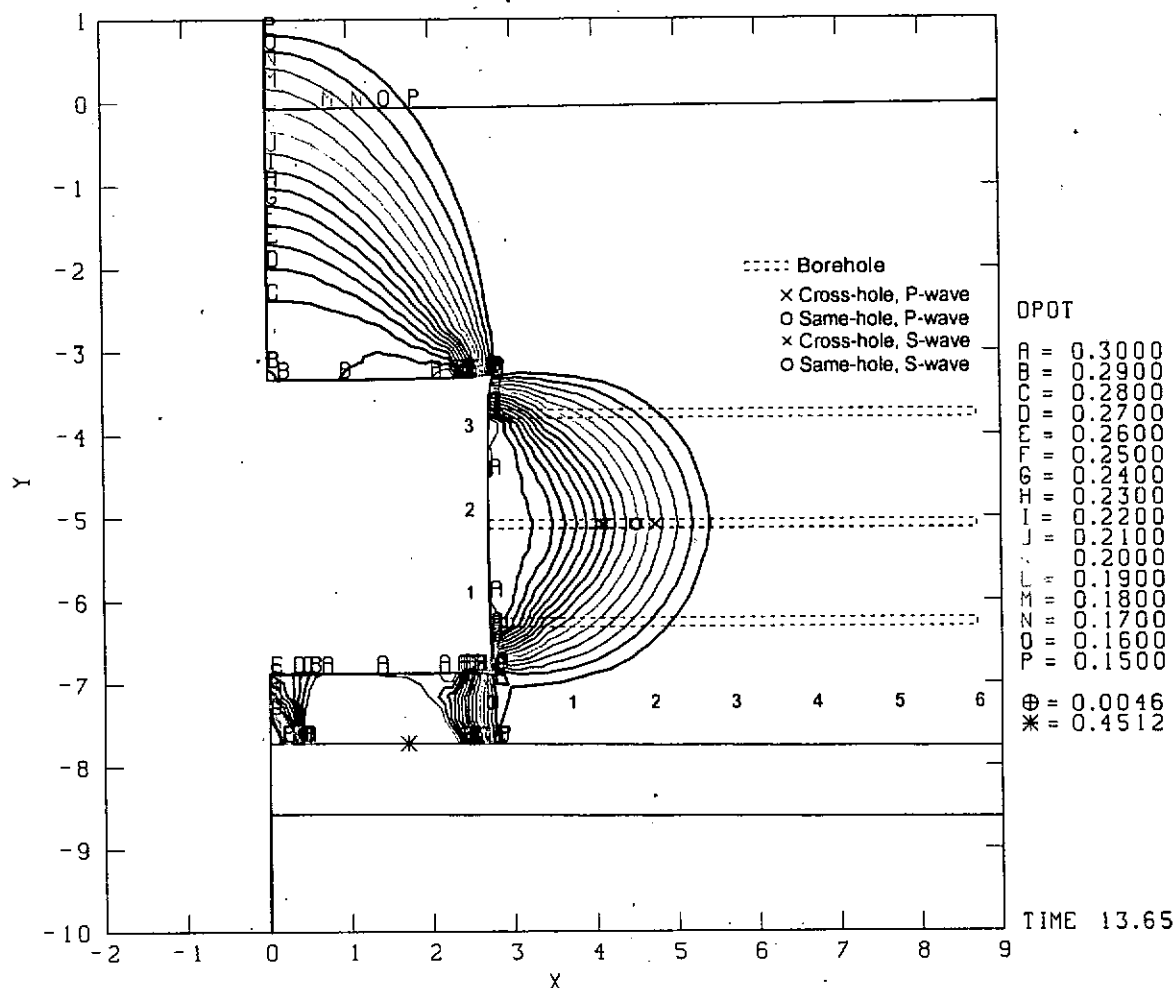
Figure 15: Damage potential contours around S-90 drift at Location 1 including ultrasonic velocity data points, which infer DRZ extent, acquired during Aug. 2001 (X- and Y-axes in m).

Table 4 lists C values corresponding to the inferred DRZ depths. Sheet ID indicates the spread sheet names in the Excel file 'Ultrasonic_wave_velocity_data_for_Room_Q_access_drift.xls', where the calculations were performed. The Excel file will be stored in the directory of 'Tests/Support/DRZ' in Concurrent Version System (CVS) as will be described in Section 5. The first and second numbers in Sheet ID indicate the borehole identification number in which a transmitter and a receiver were installed, respectively. Where the first and second numbers are the same, a transmitter and a receiver were installed in the same hole. Figure 3 shows the arrangement and naming scheme for measurement holes on the south rib of the S-90 drift. The third number indicates the year data were acquired (0 and 1 indicate 2000 and 2001, respectively). The fourth element in the Sheet ID is a letter indicating the ultrasonic wave type used for measuring the velocity (P and S mean P-wave and S-wave, respectively).

The average DPOT is calculated to be approximately 0.19. Therefore the constant, C, in the dilatant damage criterion is determined to be 0.19 rather than 0.27 which was the value used in the Clay Seam G analysis [Park and Holland, 2006] for calculating the extent of DRZ. The smaller value of C corresponds to a larger DRZ extent.

Table 4: Inferred DRZ depth and the corresponding C values.

	Excavation Date	1/15/1988			
	Date Data was acquired	5/23/2000		8/29/2001	
	Years since Excavation	12.34		13.65	
	Sheet ID	Inferred DRZ Depth (m)	Corresponding C	Inferred DRZ Depth (m)	Corresponding C
Upper Boreholes	11-10-0-P	1.105	0.180		
	12-11-0-P	1.113	0.180		
	12-12-0-S	1.562	0.160		
Middle Boreholes	13-15-1-P			2.028	0.186
	14-13-0-P	1.876	0.178		
	14-14-0-P	1.815	0.181		
	14-14-1-P			1.809	0.201
	14-14-0-S	1.929	0.174		
	14-14-1-S			1.796	0.202
	14-15-0-P	1.719	0.189		
	14-15-1-P			1.390	0.233
	14-15-1-S			1.407	0.230
Lower Boreholes	17-16-0-P	1.002	0.200		
	17-17-0-P	1.177	0.189		
	17-18-0-P	1.440	0.175		
	Average C	0.19			

3.8 DRZ Extent

Given the revised value of C, the extent of the DRZ can be assessed by determining the damage factor (D) contour in Equation (1) and the data obtained from the Clay Seam G analyses [Park and Holland, 2004]. The Clay Seam G analyses were carried out to a simulation time of 10,000 years for calculating the porosity histories in a WIPP disposal room. Thirteen cases of gas generation were investigated, these were for f=0.0, 0.025, 0.05, 0.1, 0.2, 0.4, 0.5, 0.6, 0.8, 1.0, 1.2, 1.6, and 2.0. Two cases of f=0.0 and f=1.2 are selected among them to illustrate the DRZ extent around the room. The first case, f=0.0, i.e., no gas generation, was selected as the factor which will produce the largest DRZ. The second case, f=1.2, i.e., significant gas generation, was selected as the closest factor greater than the maximum (1.123) as calculated by Herrick et al. [2007]. To calculate the damage factor contours, the results from Clay Seam G analyses were post-processed using ALGEBRA and BLOT scripts to represent Equation (1). The post-processing ALGEBRA and BLOT scripts are provided in Appendix C.

Figure 16 and Figure 17show the change with time of the DRZ around a disposal room for the gas generation factors f=0.0 and 1.2. The violet zone in the figures is defined by $D \geq 1$ in Equation (1), that is, when the dilatancy damage criterion does not predict damage in the salt. The most extensive DRZ occurs during early times, within the first ten years after the opening is mined. As the back stress from the waste stack's resistance to deformation increases, the damage to the salt as predicted by the stress invariant criterion becomes less and less.

The dilatancy damage criterion (Equation 1) no longer predicts a disturbed zone after 199 years for f=0.0 as shown in Figure 16 and after 73 years for f=1.2 as shown in Figure 17. The DRZ extents are larger than those founded in the Clay Seam G analyses [Park and Holland, 2006] because the value of C (0.19) used in this analysis is smaller than that (0.27) used in Clay Seam

G analyses. Since the value of 0.19 is obtained from the field-measured ultrasonic wave velocity test data, the results in this report are closer to the actual state.

The maximum extent of the DRZ calculated for both gas generation cases reaches approximately 1.4 m, the distance to the anhydrite layer (MB 139), below the room. The DRZ does not extend through the anhydrite layer, which acts as a buffer. The anhydrite layer should be included in the DRZ. Therefore the thickness of DRZ below the room is 2.24 m.

For both cases, the maximum extent of DRZ above the room calculated reaches to the anhydrite "a". The DRZ does not extend through the anhydrite layer, in a manner similar to what happens below the room. Thus the thickness of DRZ above the room is 4.74 m. The dilatancy damage criterion becomes satisfied ($D \geq 1$) above the room within a short period once the back of room contacts the waste. The dilatancy criterion in both the back and floor is expected to be satisfied after 120 years.

The maximum DRZ in the side of the room is calculated to be roughly 2 m. It is in the side that the dilatancy damage criterion predicts disturbance in the salt until 199 years for $f=0.0$ and 73 years for $f=1.2$.

Figure 16: Prediction of areas around a disposal room for gas generation f=0.0 (no gas pressure generated by waste) in which the dilatancy criterion is not satisfied (D < 1) with C = 0.19. (X- and Y- axes in m).
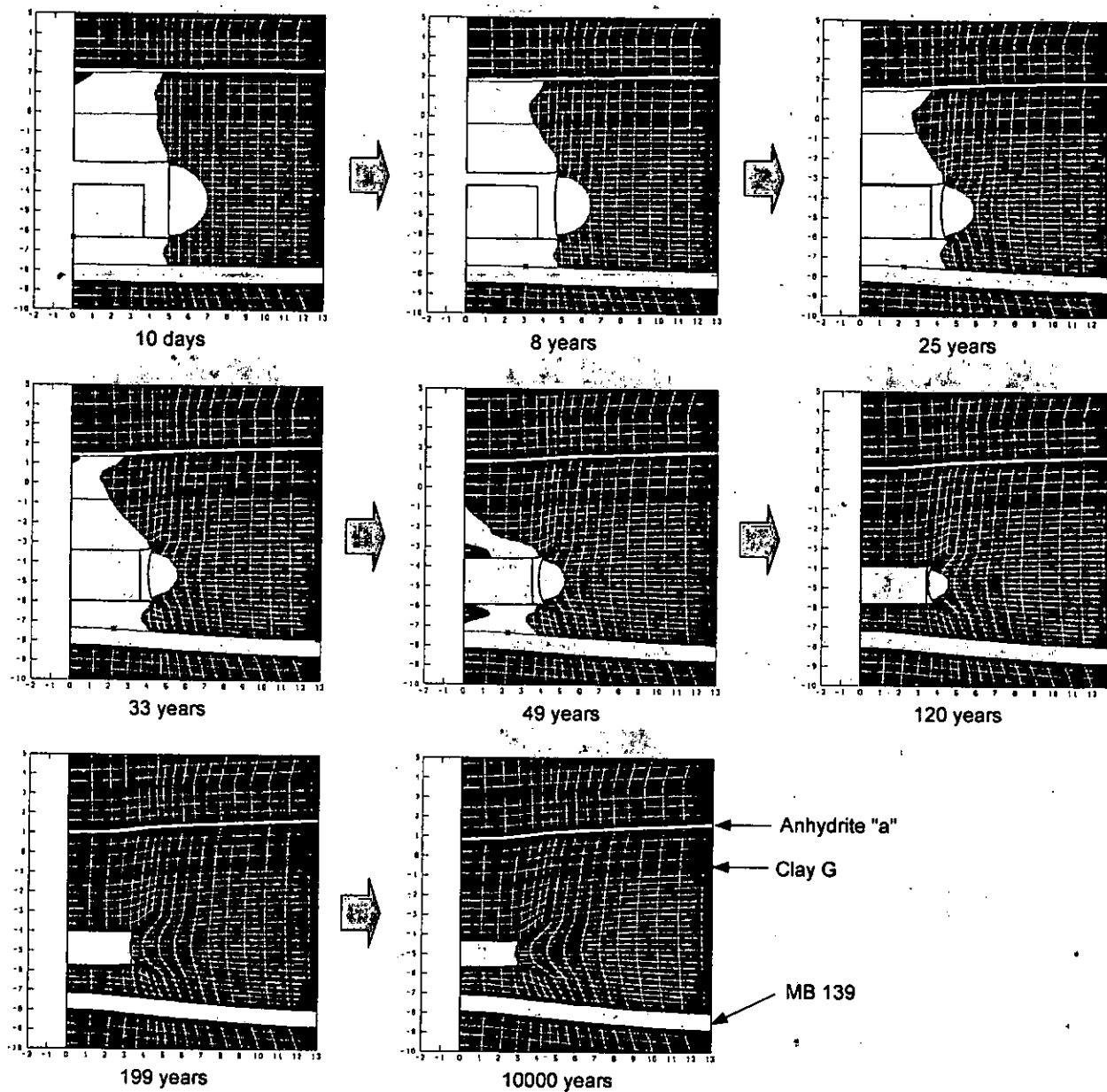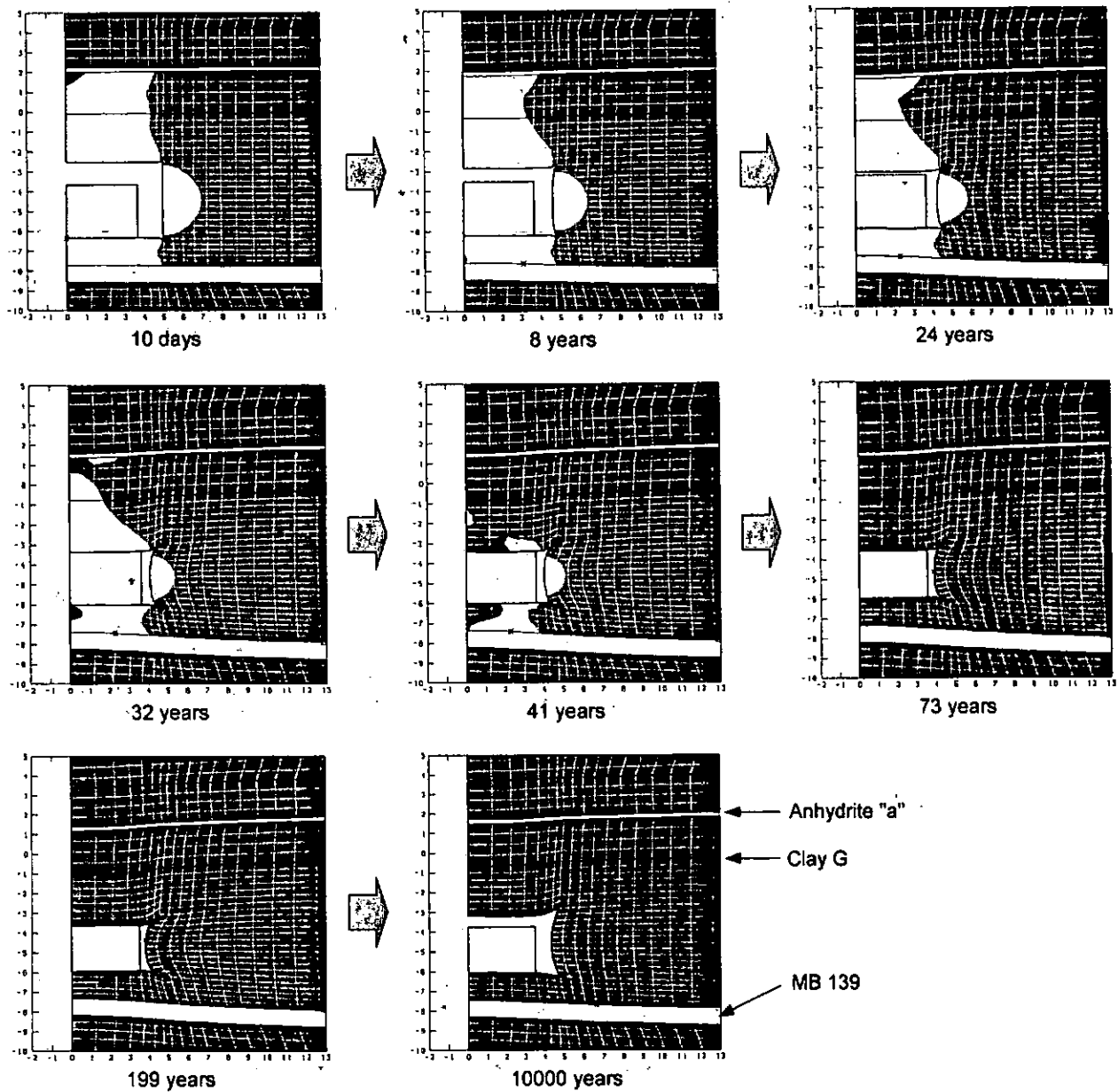
**Figure 17: Prediction of areas around a disposal room for gas generation *f*=1.2
(significant gas pressure generated by waste) in which the dilatancy criterion
is not satisfied (*D* < 1) with *C* = 0.19. (X- and Y- axes in m)**

4 PERMEABILITY OF THE DRZ

4.1 Permeability Distribution around a Disposal Room

The dilatant volumetric strains were converted to permeability using the Peach model as described in Section 2.4. The Equation (5) can be rewritten as:

$$k_p = C_p \cdot \varepsilon_V{}^3 \quad\text{..(18)}$$

where k_p is the permeability in the Peach model, C_p is a regression constant, and ε_V is the volumetric strain or dilatation which can be expressed as follows [Chen and Han, 1995]:

$$\varepsilon_V = \varepsilon_{xx} + \varepsilon_{yy} + \varepsilon_{zz} \quad\text{..(19)}$$

where the subscripts xx, yy, and zz indicate the x-directional, y-directional, and z-directional strains, respectively. The regression constant, C_p, for WIPP salt was determined by Pfeifle et al. [1998] to be $2.13 \times 10^{-8} \ m^2$.

To calculate the theoretically possible permeability distribution around a disposal room using the Peach model, the strains around the room from Clay Seam G analyses were post-processed using an ALGEBRA script which represents Equation (18). The ALGEBRA script is provided in Appendix C. The two cases of the gas generation factors, $f=0.0$ and $f=1.2$, are selected among thirteen cases as mentioned in Section 3.8 to illustrate the permeability distribution.

It is important to understand that the theoretically possible permeability change according to the Peach model is due to the formation and growth of microfractures in the rock. In the area outside of the DRZ, the ultrasonic velocity data implies that there is no increase in fracturing of the rock. Therefore, the assumption is made that the permeability in the rock beyond the DRZ is the same as the permeability of the undisturbed country rock in spite of it undergoing some volumetric strain. Therefore, this present analysis is only concerned with what is taking place within the maximum extent of the DRZ as determined in the previous section.

Figure 18 and Figure 19 show the theoretically possible change of the permeability distribution around a disposal room for the gas generation factor, $f=0.0$ and $f=1.2$, respectively. The tendency of the both distributions is similar until 32 years, at which time the back touches the top of waste. After that, the permeability for $f=1.2$ decreases faster than that for $f=0.0$ because the backpressure on the boundary of room for $f=1.2$ is larger than that for $f=0.0$. We are concerned with the permeability changes within the maximum extent of the DRZ throughout the life of the repository. This area is delineated in Frames 1 in Figure 18 and Figure 19.

As mentioned in Section 3.8, the DPOT criterion no longer predicts dilatancy damage after 199 years for $f=0.0$ case which is more severe than the $f=1.2$ case. The maximum permeability at 199 years for $f=0.0$ is $10^{-17.68} \ m^2$ within the DRZ.
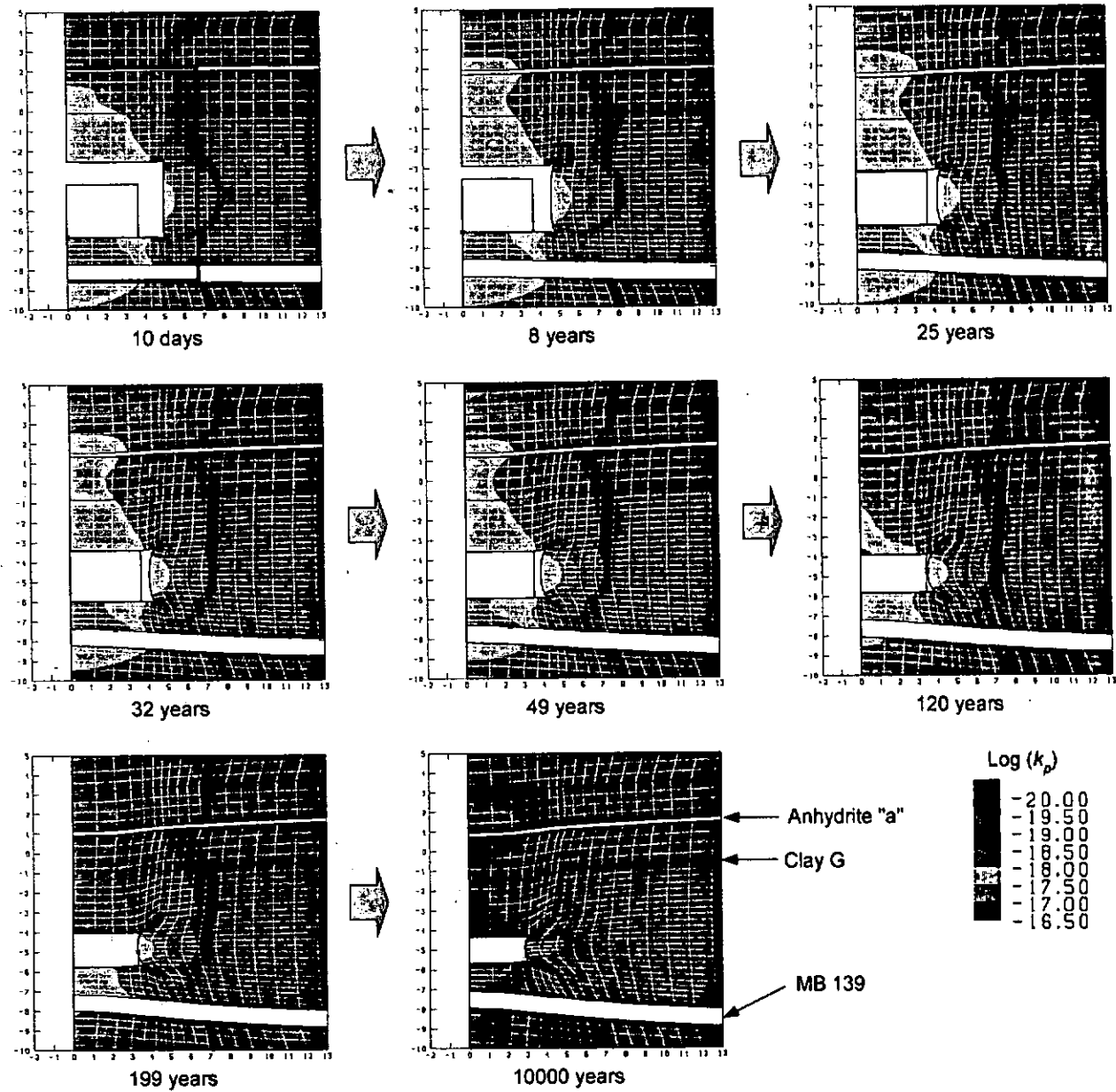
Figure 18: Change of the permeability distribution around a disposal room for gas generation factor *f*=0.0. The area of interest is the maximum extent of the DRZ which is delineated in Frame 1. (X- and Y- axes in m, k_p in m^2).
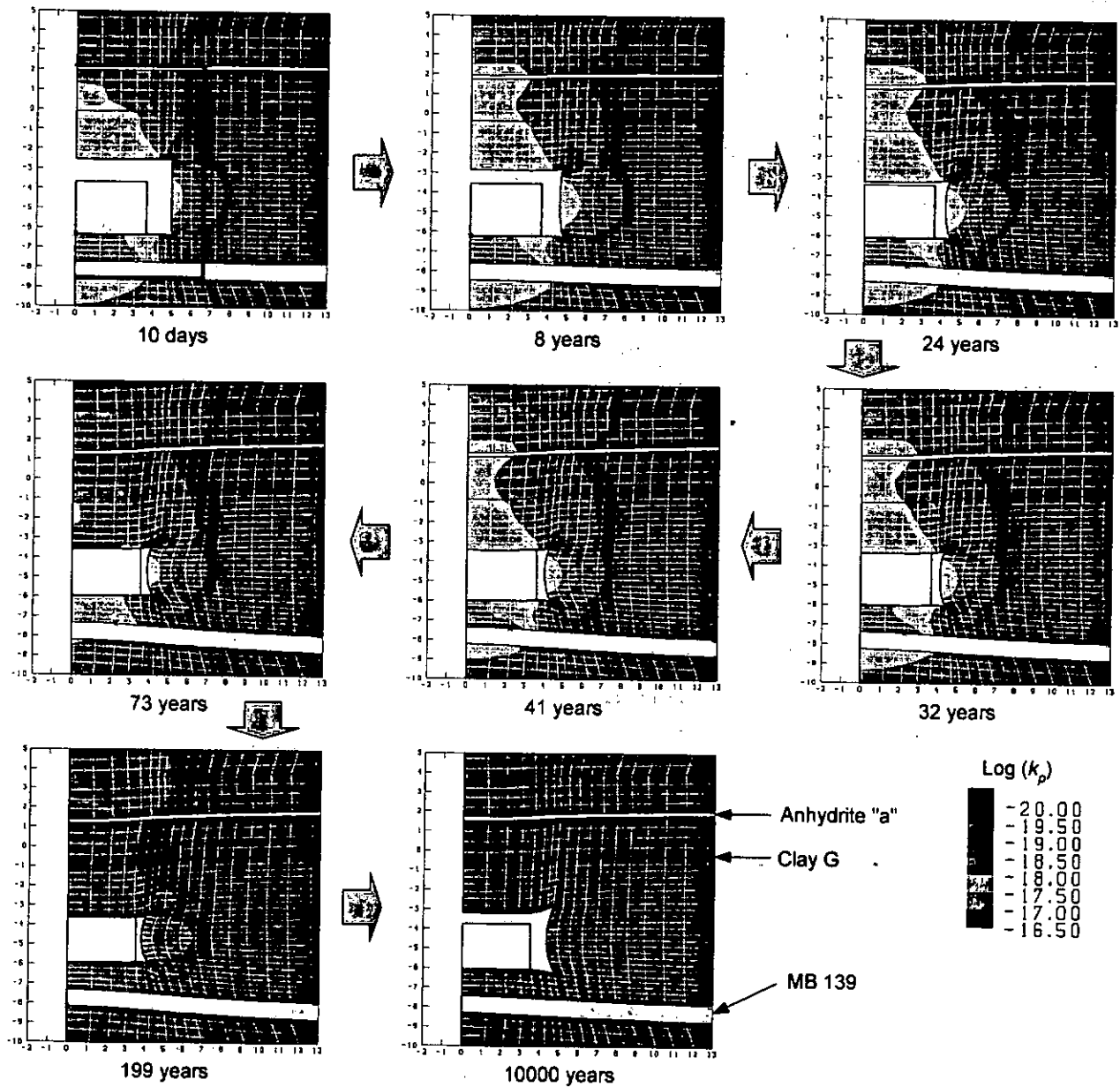
Figure 19: Change of the permeability distribution around a disposal room for gas generation factor f=1.2. The area of interest is the maximum extent of the DRZ which is delineated in Frame 1. (X- and Y- axes in m, k_p in m^2).

4.2 Properties of DRZ_2

Current WIPP PA models assume that the permeability within the DRZ around the repository rooms after closure is determined by a single, constant value for the entire 10,000-year time period simulated in BRAGFLO. However, it is known that healing in salt will occur, changing a number of physical properties in the DRZ. To accommodate this behavior in the PA models, a new material, DRZ_2 is defined. DRZ_2 more accurately reflects the behavior of the DRZ after a certain time. This section outlines the determination of the permeabilities, DRZ_2:PRMX_LOG, DRZ_2:PRMY_LOG, and DRZ_2:PRMZ_LOG, for the new material.

Examining the permeability range obtained for gas generation rates of $f = 0.0$ and $f = 1.2$, the maximum permeability in the DRZ at time $t = 200$ years after completion of excavation is calculated to be 2.09×10^{-18} m^2, while the minimum permeability is 3.24×10^{-23} m^2. In practice, however, it is difficult to measure permeabilities below about 10^{-21} m^2; additionally, the permeability of intact halite, as currently implemented in the PA Parameter Database (PDB) is from 10^{-24} m^2 to 10^{-21} m^2. Consequently, we assigned (Ismail and Park, 2007) the maximum permeability of intact halite specified in S_HALITE:PRMX_LOG, 10^{-21} m^2, as the minimum value for the permeability of the DRZ. (Although at 10,000 years after closure, the maximum value of PRMX_LOG has decreased to -18.53, we use the maximum value at 200 years after closure to establish the overall range.)

Since permeability is entered into the PA PDB as a logarithmic quantity, we treat the log of the permeability as a uniform quantity, with maximum $\log(2.09 \times 10^{-18}) = -17.68$, and minimum $\log(10^{-21}) = -21.00$. The resulting parameters are provided in the following table.

Table 5: Parameter Entry for DRZ_2 Permeabilities

Property	DRZ_2:PRMX_LOG
	DRZ_2:PRMY_LOG
	DRZ_2:PRMZ_LOG
Description	Log of intrinsic permeability, (x, y, z)-direction
Analysis	AP-133
Parameter Type	Conceptual
Distribution	Uniform
Units	m^2
Mean	−19.34
Median	−19.34
Deviation	0.958
Minimum	−21.00
Maximum	−17.68

For a uniform distribution defined along the interval $a < x < b$, both the mean and median are specified by the midpoint $c = (a + b) / 2$. For the given permeabilities, the mean and median are therefore $c = (-21.00 + -17.68) / 2 = -19.34$. The deviation is found as the square root of the variance, which is given by:

$$\sigma^2 = \int_a^b (x - \langle x \rangle)^2 p(x)dx = \left(\frac{1}{b-a}\right)\int_a^b \left(x - \frac{a+b}{2}\right)^2 dx = \frac{1}{12}(b-a)^2 \quad\quad\quad (19)$$

The deviation is therefore equal to

$$\sigma = \sqrt{\frac{(b-a)^2}{12}} = \frac{b-a}{2\sqrt{3}} = \frac{-17.68 - (-21.00)}{2\sqrt{3}} = 0.958 \quad\quad\quad (20)$$

The next step of the analysis was to find the time at which no further dilatancy of the DRZ is expected. Examining the DRZ extent graphs produced above, and using $C = 0.19$ to compute the evolution of the damage potential D with time, we find that for $t > 200$ years, essentially the

entire DRZ has $D > 1$, which indicates very little change takes place after that time. We therefore will take $t = 200$ years to be the point at which DRZ_1 is replaced by DRZ_2.

Intentionally Blank

5 COMPUTER CODES AND FILE NAMING CONVENTION

5.1 Computer Codes

The WIPP PA codes to be used for this analysis are listed in Table 6. These codes were executed on Warthog. Also used were the following commercial off-the-shelf (COTS) software, such as MATHEMATICA®, MATLAB®, MathCAD®, Excel®, Visio®, CorelDRAW®, Corel Paint Shop Pro X®, or Origin®, running on MS Windows XP®-based PC workstations and Macintosh workstations running OS X were also utilized. The use COTS application for routine calculations is justified per WIPP QA procedures NP 9-1, Appendix C and NP 19-1 as appropriate.

Table 6: Codes to be used for the revised DRZ Analysis

Code	Version	Use
APREPRO	1.78	Preprocessor
FASTQ	3.12	Mesh generation
SANTOS	2.1.7	FEM solver
ALGEBRA2	1.22	Postprocessor
BLOT II-2	1.39	Postprocessor

5.2 File Naming Convention

These calculations were performed on Sandia National Laboratories' Warthog workstation, which runs under Linux. The official runs were performed on Warthog. All the files that stored within the directory in CVS are listed and described in Table 7 through 12.

Table 7 .The command input file used was:

File	Repository	Comment
Tests/RunControl/DRZ/RS_Santos_DRZ.inp		

Table 8 .The input files used were:

File	Repository	Comment
lib/libexoIIv2c.a	ACCESS_Warthog	LIbrary used in the compilation of SANTOS
ACCESS/analysis/santos.exe/bsize.blk	ACCESS_Warthog	Include file for SANTOS subroutine compilation
bin/SSRFNT	ACCESS_Warthog	A font file for BLOT
Tests/Input/DRZ/blot_drz_lkp_curr_1p2.i	SANTOS_Analysis	Blot input file
lib/libsuplib.a	ACCESS_Warthog	LIbrary used in the compilation of SANTOS
lib/libnetcdf.a	ACCESS_Warthog	LIbrary used in the compilation of SANTOS
bin/ROMFNT	ACCESS_Warthog	A font file for BLOT
Tests/Input/DRZ/drz_lkp.alg	SANTOS_Analysis	Algebra input file
Tests/Input/DRZ/blot_drz_lkp_rais_1p2.i	SANTOS_Analysis	Blot input file
ACCESS/analysis/santos.exe/precision.blk	ACCESS_Warthog	Include file for SANTOS subroutine compilation
lib/libnemIc.a	ACCESS_Warthog	LIbrary used in the compilation of SANTOS
bin/blot.cps	ACCESS_Warthog	Postscript driver for blot
bin/grfenv.csh	ACCESS_Warthog	
	ACCESS_Warthog	Include file for SANTOS subroutine

File	Repository	Comment
ACCESS/analysis/santos.exe/timer.blk		compilation
config/site.def	ACCESS_Warthog	File used to verify path to ACCESS directories
Tests/Input/DRZ/blot_drz_lkp_curr_0p0.i	SANTOS_Analysis	Blot input file
ACCESS/analysis/santos.exe/params.blk	ACCESS_Warthog	Include file for SANTOS subroutine compilation
bin/santos.exe.o	ACCESS_Warthog	
Tests/Input/DRZ/initst_0p0.f	SANTOS_Analysis	The source code for the user-defined subroutine
bin/STKFNT	ACCESS_Warthog	A font file for BLOT
data/bypark/clayg/current/clayg0p0.e	Santos	Santos results
data/bypark/clayg/raised/clayg0p0.e	Santos	Santos results
data/bypark/clayg/raised/clayg1p2.e	Santos	Santos results
lib/libnemIf.a	ACCESS_Warthog	LIbrary used in the compilation of SANTOS
bin/algebra2	ACCESS_Warthog	Manipulate data by evaluating algebraic expressions
bin/fastq.x11	ACCESS_Warthog	Finite element 2D mesh generation program
data/bypark/clayg/current/clayg1p2.e	Santos	Santos results
bin/ex1ex2v2.exe	ACCESS_Warthog	Converts Exodus I files to Exodus II files
lib/libsantos.exe.a	ACCESS_Warthog	LIbrary used in the compilation of SANTOS
ACCESS/analysis/santos.exe/psize.blk	ACCESS_Warthog	Include file for SANTOS subroutine compilation
Tests/Input/DRZ/rqad0p0.i	SANTOS_Analysis	Santos input file
lib/libsupesdp.a	ACCESS_Warthog	LIbrary used in the compilation of SANTOS
Tests/Input/DRZ/seven.cps	SANTOS_Analysis	Blot input file
Tests/Input/DRZ/RQADrift.fsq	SANTOS_Analysis	Fatstq input file
ACCESS/analysis/santos.exe/contrl.blk	ACCESS_Warthog	Include file for SANTOS subroutine compilation
Tests/Input/DRZ/dpot.alg	SANTOS_Analysis	Algebra input file
Tests/Input/DRZ/blot_dpot_2000.i	SANTOS_Analysis	Blot input file
Tests/Input/DRZ/blot_drz_lkp_rais_0p0.i	SANTOS_Analysis	Blot input file
Tests/Input/DRZ/blot_dpot_2001.i	SANTOS_Analysis	Blot input file
bin/algebra.exe	ACCESS_Warthog	Manipulates EXODUS finite element output data by evaluating expressions
lib/libexolIv2for.a	ACCESS_Warthog	LIbrary used in the compilation of SANTOS

Table 9 .The libraries used were:

File		Comment
Santos		
SANTOS_Analysis		
ACCESS_Warthog		
SANTOS_Analysis		

Table 10 .The log file used was:

File	Repository	Comment
Tests/RunControl/LogFiles/DRZ/RS_Santos_DRZ.log	SANTOS_Analysis	ReadScript.py log file

Table 11 .The output files used were:

File	Repository	Comment

Tests/Output/DRZ/drz_lkp_curr_1p2.ps	SANTOS_Analysis	Postscript file
Tests/Output/DRZ/rqad0p0.e	SANTOS_Analysis	Santos results
Tests/Output/DRZ/drz_lkp_rais_1p2.ps	SANTOS_Analysis	Postscript file
Tests/RunControl/LogFiles/DRZ/RS_Santos_DRZ.rtf	SANTOS_Analysis	Formatted version of ReadScript.py log file
Tests/Output/DRZ/drz_lkp_rais_0p0.ps	SANTOS_Analysis	Postscript file
Tests/Output/DRZ/santos.exe	SANTOS_Analysis	
Tests/Output/DRZ/dpot0p0_2000.ps	SANTOS_Analysis	Postscript file
Tests/Output/DRZ/dpot0p0_2001.ps	SANTOS_Analysis	Postscript file
Tests/Output/DRZ/rqad0p0.ed	SANTOS_Analysis	Algebra results
Tests/Output/DRZ/drz_lkp_curr_0p0.ps	SANTOS_Analysis	Postscript file

Table 12 .The executable files used were:

File	Repository	Comment
bin/exotstv2	ACCESS_Warthog	Determines the format of an Exodus file
bin/aprepro	ACCESS_Warthog	An algebraic preprocessing program
bin/blotII2.x11	ACCESS_Warthog	Graphics code for examining meshes
bin/options	ACCESS_Warthog	Parses the options passed to the various scripts
etc/fastq	ACCESS_Warthog	The FASTQ script
etc/blot	ACCESS_Warthog	The BLOT script
etc/algebra	ACCESS_Warthog	The ALGEBRA script
etc/ex2ex1v2	ACCESS_Warthog	The ex2ex1v2 script
etc/ex1ex2v2	ACCESS_Warthog	The ex1ex2v2 script
bin/blotII2.cps	ACCESS_Warthog	Postscript driver for blot
etc/santos	ACCESS_Warthog	The SANTOS script

Intentionally Blank

6 DISCUSSION AND CONCLUDING REMARKS

The DRZ is an important feature that is included in the WIPP PA process models to predict future repository conditions and brine flow to the accessible environment. The primary purpose of this analysis is to determine the parameter values related to the DRZ around a disposal room for use in BRAGFLO analyses. The DRZ dimensions and permeability ranges used for PAVT and PABC has been overestimated. Field measurements, laboratory observations, numerical modeling, and operational experience so far show that the extent, porosity, and permeability of the DRZ can be more accurately represented.

In this analysis, the maximum extents of DRZ above and below the room are predicted to be 4.74 m and 2.24 m respectively. These values will be used for constructing the BRAGFLO grid (Figure 20). The dilatancy damage potential 200 years when the standard waste is disposed in the room. The properties of a new material to be called DRZ_2, which reflects the long-term physical properties of salt of the DRZ after healing has taken place, are determined from this analysis. The parameters of DRZ_2:PRXM_LOG, DRZ_2:PRMY_LOG, and DRZ_2:PRMZ_LOG have a uniform distribution with the mean and median value of -19.34, the deviation of 0.958, the maximum value of -17.68, and the minimum value of -21.00. This distribution has been provided to the BRAGFLO analysis team.

During the analysis, the constant, C, in the dilatancy criterion was determined to be 0.19, which is based on the ultrasonic velocity data measured at Location 1 within the WIPP S-90 drift. This value is less then 0.27 which was determined by van Sambeek, et al. [1993] during laboratory testing. The smaller value of C predicts a larger DRZ extent. The C value developed in this analysis is believed to be more representative of the actual field value because of the large number of sensitive DRZ depth measurements in a WIPP drift used.
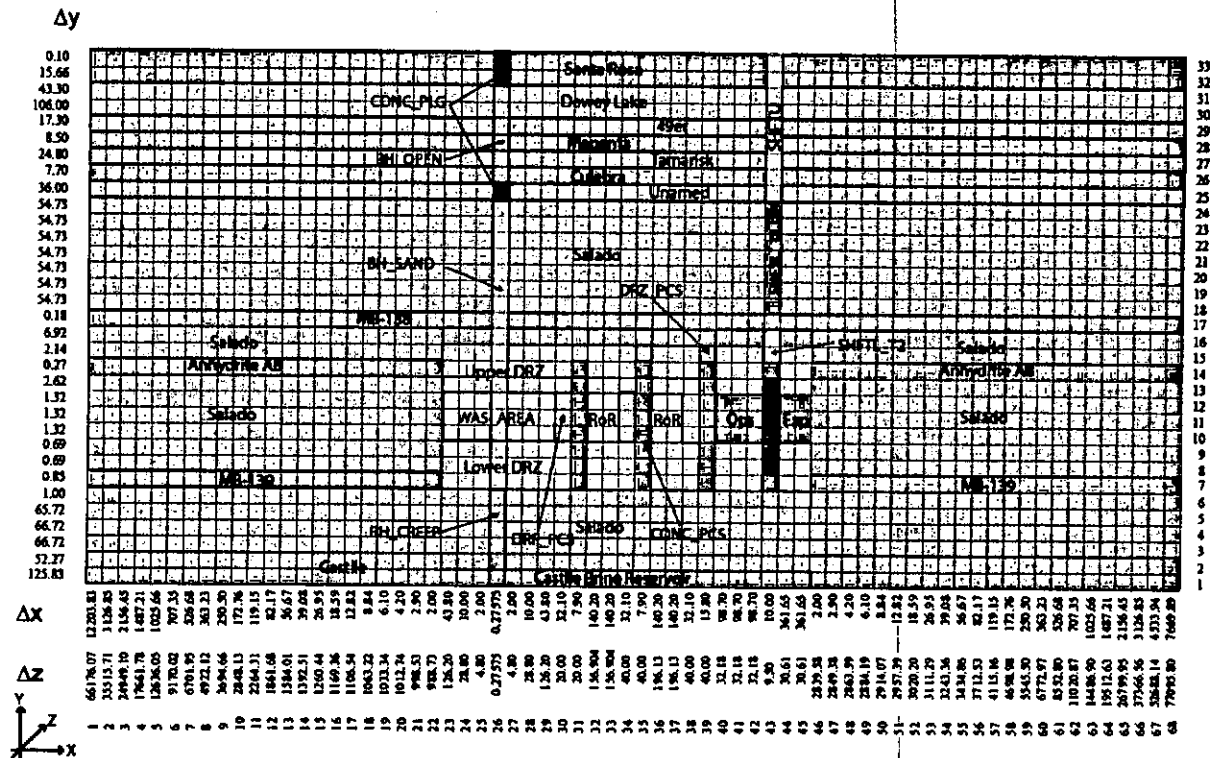

Figure 20: Revised BRAGFLO grid.

Intentionally Blank

7 REFERENCES

Butcher, B.M. 1997. *A Summary of the Sources of Input Parameter Values for the WIPP Final Porosity Surface Calculations*, SAND97-0796, Albuquerque, NM: Sandia National Laboratories.

Carman, P. C. 1937. Fluid flow through granular beds. *Trans. Inst. Chem. Eng. London.* Vol. 15, 150-166.

Chan, K. S., S. R. Bodner and D. E. Munson. 2001. Permeability of WIPP Salt during Damage Evolution and Healing, *Int. J. Damage Mech.* Vol. 10, 347-375.

Chen, W.F. and Han, D.J., 1995. Plasticity for Structural Engineers, Taipei, Taiwan: Gau Lih Book Co.

Domski, P.S., D.T. Upton and R.L. Beauheim, 1996. *Hydraulic Testing around Room Q: Evaluation of the Effects of Mining on the Hydraulic Properties of Salado Evaporites*, SAND96-0435, Sandia National Laboratories, Albuquerque, NM.

Goodman, R. E., 1989, *Introduction to Rock Mechanics, 2nd Edition,* John Wiley & Sons.

Hansen, F. D., 2003. *The Disturbed Rock Zone at the Waste Isolation Pilot Plant.* SAND2003-3407, Sandia National Laboratories, Albuquerque, NM.

Herrick, C.G., M. Riggins, and B.Y. Park. 2007. *Recommendation for the Lower Limit of the Waste Shear Strength (Parameter BOREHOLE : TAUFAIL).* Sandia National Laboratories, Carlsbad, NM. ERMS 546033.

Holcomb, D. and R. Hardy, 2001. *Status of Ultrasonic Wave Speed Measurements Undertaken to Characterize the DRZ in the Assess Drift to Q Room*, Memorandum to F. Hansen, Sandia National Laboratories, dated January 22, 2001.

Ismail, A.E., and B.Y. Park, 2007. *Revised Permeability Estimates for the Disturbed Rock Zone (DRZ)*, Memorandum to E.D. Vugrin, Sandia National Laboratories, dated April 2, 2007. ERMS 545746.

Jaeger, J. C. and N. G. W. Cook, 1979. *Fundamentals of Rock Mechanics (3rd Ed)*, 84-86, Chapman and Hall, New York.

Leigh, C. D., J. F. Kanney, L. H. Brush, J. W. Garner, R. Kirkes, T. Lowry, M. B. Nemer, J. S. Stein, E. D. Vugrin, S. Wagner, and T. B. Kirchner. 2005. *2004 Compliance Recertification Application Performance Assessment Baseline Calculation, Revision 0.* Carlsbad, NM: Sandia National Laboratories. ERMS 541521.

MacDonald, T. 2000. *Duke University Connexes Installation Recommendations*, Memorandum to Dennis A. Hofer, WID, dated July 18, 2000.

Munson, D.E. and P.R. Dawson. 1979. *Constitutive model for the low temperature creep of salt (with application to WIPP)*. Albuquerque, NM: Sandia National Laboratories. SAND79-1853.

Munson, D. E., and P. R. Dawson, 1982. *A Transient Creep Model for Salt during Stress Loading and Unloading*, SAND82-0962, Albuquerque, NM: Sandia National Laboratories.

Munson, D.E. and P.R. Dawson. 1984. Salt constitutive modeling using mechanism maps. In *The Mechanical Behavior of Salt, Proceedings of the First Conference, Pennsylvania State University, University Park, PA, November 9-11, 1981*, eds. H.R. Hardy, Jr. and M. Langer, 717-737. Rockport, MA: Karl Distributors

Munson, D. E., A. F. Fossum and P. E. Senseny, 1989. *Advances in Resolution of Discrepancies between Predicted and Measured, In Situ Room Closures*, SAND88-2948, Albuquerque, NM: Sandia National Laboratories.

Park, B. Y., 2002. *Analysis Plan for the Structural Evaluation of WIPP Disposal Room raised to Clay Seam G*, AP-093, Revision 1, Sandia National Laboratories, Carlsbad, NM.

Park, B. Y. and A. E. Ismail, 2007. *Analysis Plan for Prediction of the Extent and Permeanility of the Disturbed Rock Zone around a WIPP Disposal Room*, AP-133, Sandia National Laboratories, Carlsbad, NM.

Park, B. Y., and J. F. Holland. 2004. *Analysis Report for Structural Evaluation of WIPP Disposal Room Raised to Clay Seam G*, SAND2003-3409, Albuquerque, NM: Sandia National Laboratories.

Park, B. Y. and J. F. Holland. 2006. *Error in DRZ Calculation in the Clay Seam G Analysis*, Memorandum to M. Y. Lee, Sandia National Laboratories, dated December 21, 2006, ERMS 545053.

Peach, C. J. 1991. *Influence of Deformation on the Fluid Transport Properties of Salt Rocks*, Ph.D. Thesis, Department of *Geology*, University of Utrecht, Netherlands.

Pfeifle, T. W., N. S. Brodsky, and D. E. Munson. 1998. Experimental determination of the relationship between permeability and microfracture-induced damage in bedded salt. SAND98-0411C. *Proposed for presentation at the 3rd North American Rock Mechanics Symposium held June 3-5, 1998 in Cancun, Mexico*, 10 p.

Powers, D. W., 2000. Task 2, contract 5987 (WIPP Underground Test Site Selection and Description), Memorandum to J.S. Rath, Sandia National Laboratories, dated March 31, 2000.

Stone, C. M., 1997a. *Final Disposal Room Structural Response Calculations*, SAND97-0795, Sandia National Laboratories, Albuquerque, NM.

Stone, C.M., 1997b. *SANTOS-A Two-Dimensional Finite Element Program for the Quasistatic, Large Deormation, Inelastic Response of Solids*, SAND90-0543, Sandia National Laboratories, Albuquerque, NM.

Stormont, J. C., 1990. *Gas Permeability Changes in Rock Salt during Deformation*, Ph.D. Thesis, University of Arizona, Tucson AZ.

Van Sambeek, L., J. Ratigan, and F. Hansen, 1993. *Dilatancy of Rock Salt in Laboratory Tests*, Proc. 34th U.S. Symposium on Rock Mechanics, p.245-248.

WIPP PA (Performance Assessment), 2003. *Verification and Validation Plan/Validation Document for SANTOS 2.1.7.*, Carlsbad, NM: Sandia National Laboratories, Sandia WIPP Central Files ERMS # 530091.

WTS (Washington TRU Solutions), 1994. S90 As-built Survey September 1993 & September 1994, Mine Engineering Departments.

Intentionally Blank

APPENDIX A: FASTQ INPUT FILE

```
TITLE
Room Q Access Drift Model - 2D (B.Y.Park, 2/14/2007)
$
$ Define Points
$         ID      X         Y
POINT    10      0.00      52.87
POINT   100     50.00      52.87
POINT    11      0.00      49.38
POINT   110     50.00      49.38
POINT    12      0.00      31.86
POINT   120     50.00      31.86
POINT    13      0.00      28.30
POINT   130     50.00      28.30
POINT    14      0.00       9.35
POINT   145      2.82       9.35
POINT   140     50.00       9.35
POINT    15      0.00       9.16
POINT   155      2.82       9.16
POINT   150     50.00       9.16
POINT    16      0.00       4.27
POINT   165      2.82       4.27
POINT   160     50.00       4.27
POINT    17      0.00       2.31
POINT   175      2.82       2.31
POINT   170     50.00       2.31
POINT    18      0.00       2.10
POINT   185      2.82       2.10
POINT   180     50.00       2.10
POINT    19      0.00       0.00
POINT   195      2.82       0.00
POINT   190     50.00       0.00
POINT    20      0.00      -3.21
POINT   205      2.82      -3.21
POINT   200     50.00      -3.21
POINT    21      0.00      -6.93
POINT   215      2.82      -6.93
POINT   210     50.00      -6.93
POINT    22      0.00      -7.77
POINT   225      2.82      -7.77
POINT   220     50.00      -7.77
POINT    23      0.00      -8.63
POINT   235      2.82      -8.63
POINT   230     50.00      -8.63
POINT    24      0.00     -26.21
POINT   240     50.00     -26.21
POINT    25      0.00     -30.61
POINT   250     50.00     -30.61
POINT    26      0.00     -54.19
POINT   260     50.00     -54.19
$
$ Define Lines
$$ Left Vertical Lines
$         ID    Type   Point          intvls  increment
LINE     10     STR    10    11    0    1
LINE     11     STR    11    12    0    5
LINE     12     STR    12    13    0    1
LINE     13     STR    13    14    0    {n13= 8} {i13=0.88}
LINE     14     STR    14    15    0    1
LINE     15     STR    15    16    0    6
LINE     16     STR    16    17    0    4
LINE     17     STR    17    18    0    1
LINE     18     STR    18    19    0    4
LINE     19     STR    19    20    0    {n19= 8} {i19=0.9}  $ Right above drift
LINE     20     STR   205   215    0    {n20=12}            $ Drift wall
LINE     21     STR    21    22    0    {n21= 3}            $ Right below drift
LINE     22     STR    22    23    0    {n22= 3}            $ MB139
LINE     23     STR    23    24    0    {n23=16} {i23=1.11} $ Right below MB139
LINE     24     STR    24    25    0    2
LINE     25     STR    25    26    0    {n25= 7} {i25=1.1}
$$ Right Vertical Lines
LINE    100     STR   100   110    0    1
LINE    110     STR   110   120    0    5
LINE    120     STR   120   130    0    1
```

```
LINE    130      STR    130   140     0     {n13} {i13}
LINE    140      STR    140   150     0     1
LINE    150      STR    150   160     0     6
LINE    160      STR    160   170     0     4
LINE    170      STR    170   180     0     1
LINE    180      STR    180   190     0     4
LINE    190      STR    190   200     0     {n19} {i19}
LINE    200      STR    200   210     0     {n20}
LINE    210      STR    210   220     0     {n21}
LINE    220      STR    220   230     0     {n22}
LINE    230      STR    230   240     0     {n23} {i23}
LINE    240      STR    240   250     0     2
LINE    250      STR    250   260     0     {n25} {i25}
$$ Horizontal Lines
$ number of intervals in drift:  {nd=10}
$ increment in drift:            {id=1.0}
$ number of intervals in pillar:{np=26}
$ increment in pillar:           {ip=1.12}
$ increment for mitigation 1    :{im1=1.06}
$ increment for mitigation 2    :{im2=1.052}
$ increment for mitigation 3    :{im3=1.005}
LINE    1000     STR    10    100     0     {nd+np}
LINE    1100     STR    11    110     0     {nd+np} {im3}
LINE    1200     STR    12    120     0     {nd+np} {im2}
LINE    1300     STR    13    130     0     {nd+np} {im1}
LINE    1400     STR    14    145     0     {nd} {id}
LINE    1450     STR    145   140     0     {np} {ip}
LINE    1500     STR    15    155     0     {nd} {id}
LINE    1550     STR    155   150     0     {np} {ip}
LINE    1600     STR    16    165     0     {nd} {id}
LINE    1650     STR    165   160     0     {np} {ip}
LINE    1700     STR    17    175     0     {nd} {id}
LINE    1750     STR    175   170     0     {np} {ip}
LINE    1800     STR    18    185     0     {nd} {id}
LINE    1850     STR    185   180     0     {np} {ip}
LINE    1900     STR    19    195     0     {nd} {id}
LINE    1950     STR    195   190     0     {np} {ip}
LINE    2000     STR    20    205     0     {nd} {id}
LINE    2050     STR    205   200     0     {np} {ip}
LINE    2100     STR    21    215     0     {nd} {id}
LINE    2150     STR    215   210     0     {np} {ip}
LINE    2200     STR    22    225     0     {nd} {id}
LINE    2250     STR    225   220     0     {np} {ip}
LINE    2300     STR    23    235     0     {nd} {id}
LINE    2350     STR    235   230     0     {np} {ip}
LINE    2400     STR    24    240     0     {nd+np} {im1}
LINE    2500     STR    25    250     0     {nd+np} {im2}
LINE    2600     STR    26    260     0     {nd+np}
$
$ Define Side
$       ID      Line   Line
SIDE    1400     1400   1450
SIDE    1500     1500   1550
SIDE    1600     1600   1650
SIDE    1700     1700   1750
SIDE    1800     1800   1850
SIDE    1900     1900   1950
SIDE    2000     2000   2050
SIDE    2100     2100   2150
SIDE    2200     2200   2250
SIDE    2300     2300   2350
$
$ NODEBC CARDS
$$ Left
$       ID Line...
NODEBC   1 10  11  12  13  14  15  16  17  18  19     21  22  23  24  25
$$ Right
NODEBC   1 100 110 120 130 140 150 160 170 180 190 200 210 220 230 240 250
$$ Bottom
NODEBC   2 2600
$
$ SIDEBC CARDS
$       ID  Line
SIDEBC  10 1000     $ Top of Model
SIDEBC  20 2600     $ Bottom of Model
SIDEBC 100 2000     $ Drift Back
```

```
SIDEBC 200    20    $ Drift Wall
SIDEBC 300  2100    $ Drift Floor
SIDEBC 700  2100 20 2000 $ Drift Boundary
$
$ REGION CARDS
$ Block 1=Argillaceous 2=Anhydrite 3=Halite
$       ID Block   B      R      T      L
REGION  10    2 -1100   -100 -1000   -10
REGION  11    1 -1200   -110 -1100   -11
REGION  12    2 -1300   -120 -1200   -12
REGION  13    1  1400   -130 -1300   -13
REGION  14    2  1500   -140  1400   -14
REGION  15    1  1600   -150  1500   -15
REGION  16    3  1700   -160  1600   -16
REGION  17    2  1800   -170  1700   -17
REGION  18    3  1900   -180  1800   -18
REGION  19    1  2000   -190  1900   -19
REGION  20    1 -2150   -200 -2050   -20
REGION  21    1  2200   -210  2100   -21
REGION  22    2  2300   -220  2200   -22
REGION  23    1 -2400   -230  2300   -23
REGION  24    2 -2500   -240 -2400   -24
REGION  25    1 -2600   -250 -2500   -25
$
SCHEME   P
EXIT
```

APPENDIX B-1: SANTOS INPUT FILE FOR THE DRIFT ANALYSIS

```
TITLE
Prediction of DRZ around Room Q Access Drift: f=0.0
$
PLANE STRAIN
INITIAL STRESS = USER
GRAVITY = 1 = 0. = -9.79 = 0.
PLOT ELEMENT, STRESS, STRAIN, VONMISES, PRESSURE, HG, EFFMOD
PLOT NODAL, DISPLACEMENT, RESIDUAL
PLOT STATE, EQCS, EV
RESIDUAL TOLERANCE = 0.5
MAXIMUM ITERATIONS = 1000
MAXIMUM TOLERANCE = 100.
INTERMEDIATE PRINT = 100
ELASTIC SOLUTION
PREDICTOR SCALE FACTOR = 3
AUTO STEP .015 2.592E6 NOREDUCE 1.E-5
TIME STEP SCALE = 0.5
HOURGLASS STIFFENING = .005
$
STEP CONTROL
500   3.1536e7      $ 1 year
2000  3.1536e9      $ 100 years
300   3.1536e10     $ 1000 years
END
$
OUTPUT TIME
1     3.1536e7      $ 1 year
10    3.1536e9      $ 100 years
30    3.1536e10     $ 1000 years
END
$
PLOT TIME
10    3.1536e7      $ 1 year
1     6.3072e8      $ 20 years
10    3.1536e9      $ 100 years
30    3.1536e10     $ 1000 years
END
$
MATERIAL, 1, M-D CREEP MODEL, 2300. $ ARGILLACEOUS HALITE
TWO MU = 24.8E9
BULK MODULUS = 20.66E9
A1 = 1.407E23
Q1/R = 41.94
N1 = 5.5
B1 = 8.998E6
A2 = 1.314E13
Q2/R = 16.776
N2 = 5.0
B2 = 4.289E-2
SIG0 = 20.57E6
QLC = 5335.
M = 3.0
K0 = 2.47E6
C = 2.759
ALPHA = -14.96
BETA = -7.738
DELTLC = .58
RN3 = 2.
AMULT = .95
END
$
MATERIAL, 2, SOIL N FOAMS, 2300. $ ANHYDRITE
TWO MU = 5.563E10
BULK MODULUS = 8.3444E10
A0 = 2.338e6
A1 = 2.338
A2 = 0.
PRESSURE CUTOFF = 0.0
FUNCTION ID = 0
END
$
MATERIAL, 3, M-D CREEP MODEL, 2300. $ PURE HALITE
TWO MU = 24.8E9
```

```
BULK MODULUS = 20.66E9
A1 = 8.386E22
Q1/R = 41.94
N1 = 5.5
B1 = 6.086E6
A2 = 9.672E12
Q2/R = 16.776
N2 = 5.0
B2 = 3.034E-2
SIG0 = 20.57E6
QLC = 5335.
M = 3.0
K0 = 6.275E5
C = 2.759
ALPHA = -17.37
BETA = -7.738
DELTLC = .58
RN3 = 2.
AMULT = .95
END
$
NO DISPLACEMENT X = 1
NO DISPLACEMENT Y = 2
PRESSURE, 10, 1, 13.57E6
$
CONTACT SURFACE, 300, 200, 0., 1.E-3, 1.E4
CONTACT SURFACE, 100, 200, 0., 1.E-3, 1.E4
CONTACT SURFACE, 100, 300, 0., 1.E-3, 1.E4
ADAPTIVE PRESSURE, 700, 1.e-6, -6.4
$
FUNCTION,1 $ FUNCTION TO DEFINE PRESCRIBED PRESSURE
0., 1.
3.1536e11, 1.
END
$
FUNCTION = 3
0. 0.5
3.1536E11 1.
END
EXIT
```

APPENDIX B-2: CALCULATING THE SANTOS INPUT PARAMETERS

Halite Constitutive Model:

Shear Modulus (G): $\mu := 12400 \cdot MPa$ (SAND97-0796, Table 3, p.12)

Young's Modulus: $E := 31000 \cdot MPa$ (SAND97-0796, Table 3, p.12)

Poisson's ratio: $\nu := 0.25$ (SAND97-0796, Table 3, p.12)

TWO MU: $TwoMu := 2 \cdot \mu$ $TwoMu = 2.48 \times 10^{10} Pa$

Bulk Modulus: $K_B := \dfrac{E}{3 \cdot (1 - 2 \cdot \nu)}$ $K_B = 2.0667 \times 10^{10} Pa$

Creep Constant:

Universal Gas Constant: $R := 8.3144 \cdot 10^7 \cdot \dfrac{erg}{mol \cdot K}$ $1 \cdot erg = 2.3885 \times 10^{-8} cal$

Temperature: $T := 300 \cdot K$ $T = 300 K$

$Q_1 := 25000 \cdot \dfrac{cal}{mol}$ (SAND97-0796, Table 3, p.13)

$\dfrac{Q_1}{R \cdot T} = 41.9633$

$Q_2 := 10000 \cdot \dfrac{cal}{mol}$ (SAND97-0796, Table 3, p.13)

$\dfrac{Q_2}{R \cdot T} = 16.7853$

$c := 9.198 \cdot 10^{-3} \cdot \dfrac{1}{K}$ (SAND97-0796, Table 3, p.14)

$C := c \cdot T$ $C = 2.7594$

Exponent of workhardening and recovery term used to compute F: $RN3 := 2.0$

Scalar multiplier of time step needed for stability, default 0.98): $AMULT := 0.95$

(SAND90-0543, p.70)

Anhydrite Constitutive Model:

Shear Modulus (G): $\mu := 27815 \cdot MPa$ (SAND97-0796, Table 2.2, p.A-98)

Young's Modulus: $E := 75100 \cdot MPa$ (SAND97-0796, Table 2.2, p.A-98)

Poisson's ratio: $\nu := 0.35$ (SAND97-0796, Table 2.2, p.A-98)

TWO MU: $TwoMu := 2 \cdot \mu$ $TwoMu = 5.563 \times 10^{10} Pa$

Bulk Modulus: $K := \dfrac{E}{3 \cdot (1 - 2 \cdot \nu)}$ $K = 8.3444 \times 10^{10} Pa$

Elastic Constant: $C := 1.35 \cdot MPa$ (SAND97-0796, Table 1, p.B-9)

Drucker-Prager Constant: $a := 0.45$ (SAND97-0796, Table 1, p.B-9)

SANTOS Input Constant: $A0 := \sqrt{3} \cdot C$ $A0 = 2.3383 \times 10^{6} Pa$

$A1 := 3\sqrt{3} \cdot a$ $A1 = 2.3383$

$A2 := 0.0$ (SAND97-0796, Table 2, p.B-10)

APPENDIX C: ALGEBRA AND BLOT SCRIPT FOR DAMAGE POTENTIAL CONTOURS

```
==ALGEBRA=====
' Damage Potential (DPOT) Contours
' journalized by B.Y.Park on Feb. 15, 2007
'
ALLTIMES
'
' Mesh plots will be deformed
'
SAVE NODAL
'
' CONVERT STRESSES FROM PASCALS (Pa) TO MEGA-PASCALS (MPa)
'
SIGXX = SIGXX/1.0E+06
SIGYY = SIGYY/1.0E+06
SIGZZ = SIGZZ/1.0E+06
TAUXY = TAUXY/1.0E+06
VONMISES = VONMISES/1.0E+06
'
' Compute Sqrt(J2) and I1 (MPa)
' Compute mean pressure and limit it to 1.e-06
'
PRE = -( SIGXX + SIGYY + SIGZZ )/3.0
PRE1 = ABS(PRE) - 1.E-6
PRE2 = IFGZ(PRE1,PRE1,1.0E-6)
SJ2=VONMISES/SQRT(3.0)
I1=3.*PRE2
'
' compute damage potential in the halite
'
BLOCKS 1 3
DPOT = SJ2/I1
'
' Define time in terms of years
'
TIME = TIME/3.1536E7
'
' Delete unneeded variables
'
DELETE PRE, PRE1, PRE2, SJ2, I1
END

==BLOT===================================
det
times 12.36
zoom -2 9 -10 1
tic 1
contour dpot
rain 16
ncntrs 16
crange 0.3 0.15
copen off off
qa off
plot
exit
```

APPENDIX D: FIGURES FOR INFERRING THE DRZ DEPTH

Room Q Access Drift, QGU11->QGU10, P-Wave
(Data acquired on May 23 to 24, 2000)

$y = 0.300x + 4.117$

$y = 4.449$

1.105

V$_P$ (km/s)

Depth (m)
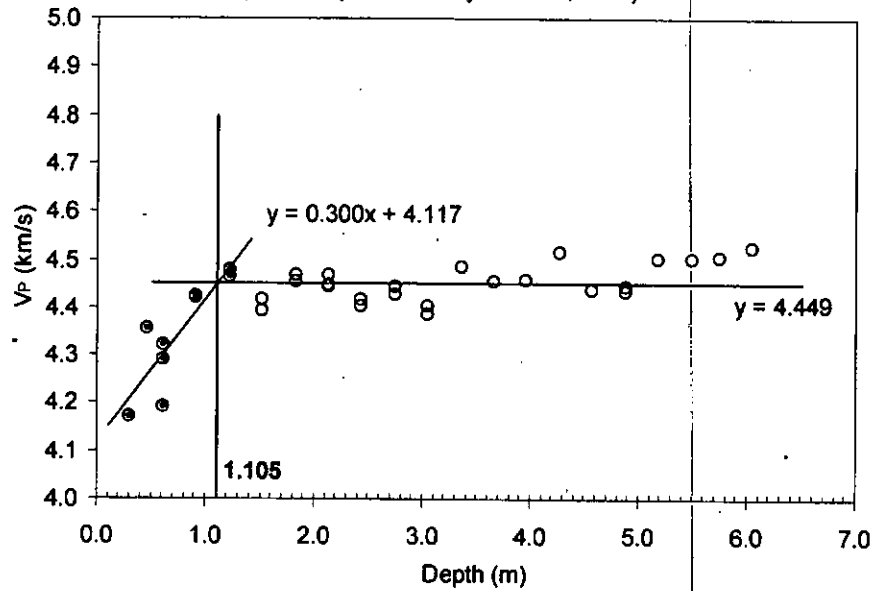
Room Q Access Drift, QGU12->QGU11, P-Wave
(Data acquired on May 24, 2000)

$y = 0.348x + 4.007$

$y = 4.394$

1.113

V$_P$ (km/s)

Depth (m)
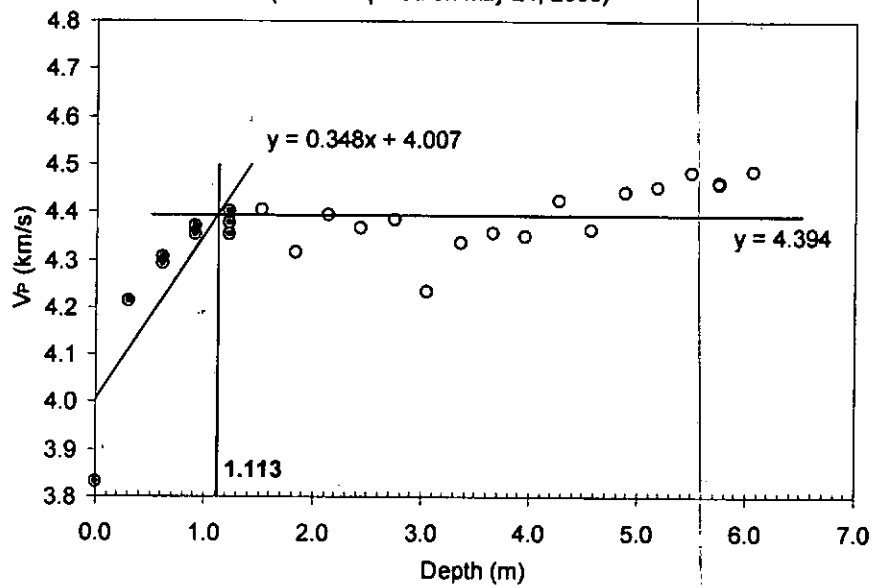
Room Q Access Drift, QGU12->QGU12, S-Wave
(Data acquired on May 24, 2000)

$y = 0.386x + 1.933$

$y = 2.536$

1.562
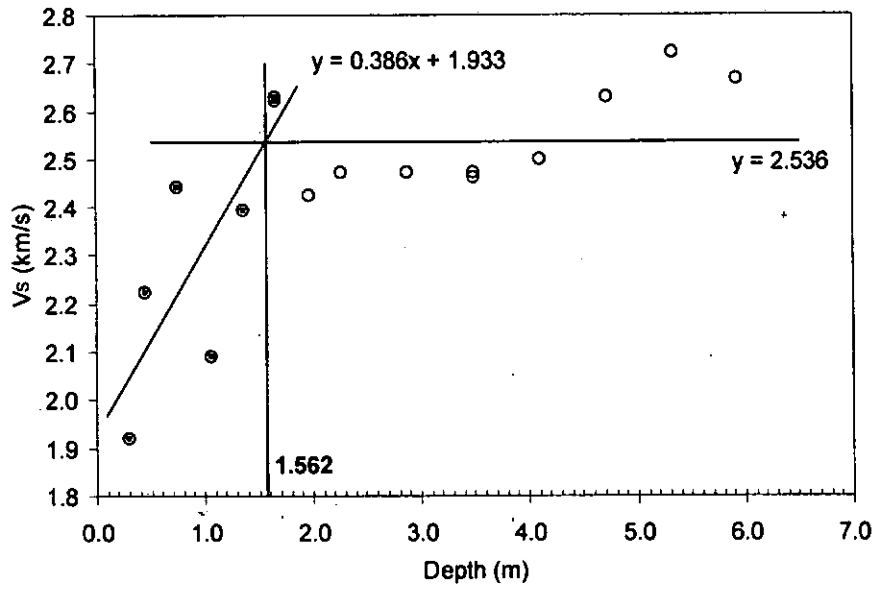
Room Q Access Drift, QGU14->QGU13, P-Wave
(Data acquired on May 25, 2000)
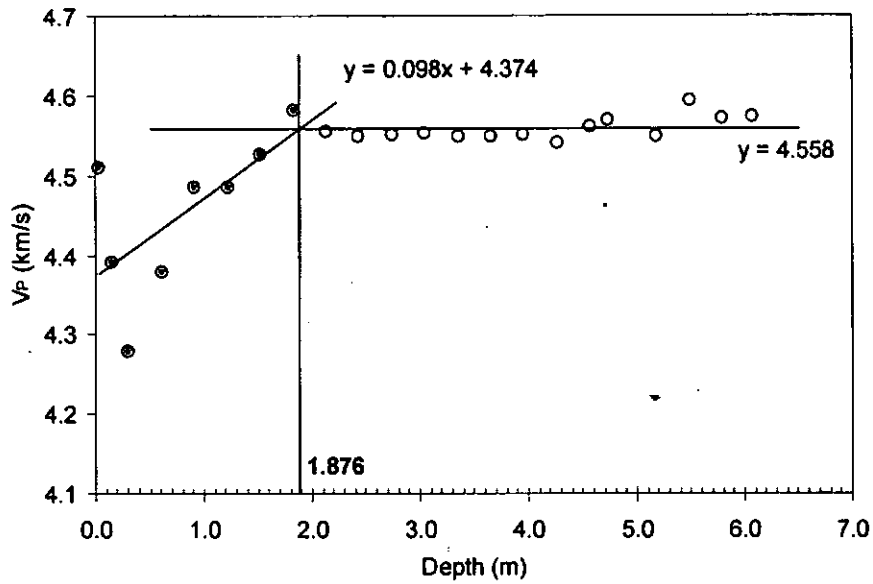
$y = 0.098x + 4.374$

$y = 4.558$

1.876

Room Q Access Drift, QGU14->QGU14, P-Wave
(Data acquired on May 25, 2000)

$y = 0.671x + 3.623$

$y = 4.841$

1.815

Vp (km/s)

Depth (m)

Room Q Access Drift, QGU14->QGU14, S-Wave
(Data acquired on May 25, 2000)

$y = 0.209x + 2.746$

$y = 3.149$

1.929

Vs (km/s)

Depth (m)

Room Q Access Drift, QGU14->QGU15, P-Wave
(Data acquired on May 25, 2000)

$y = 0.371x + 3.997$

$y = 4.635$

1.719
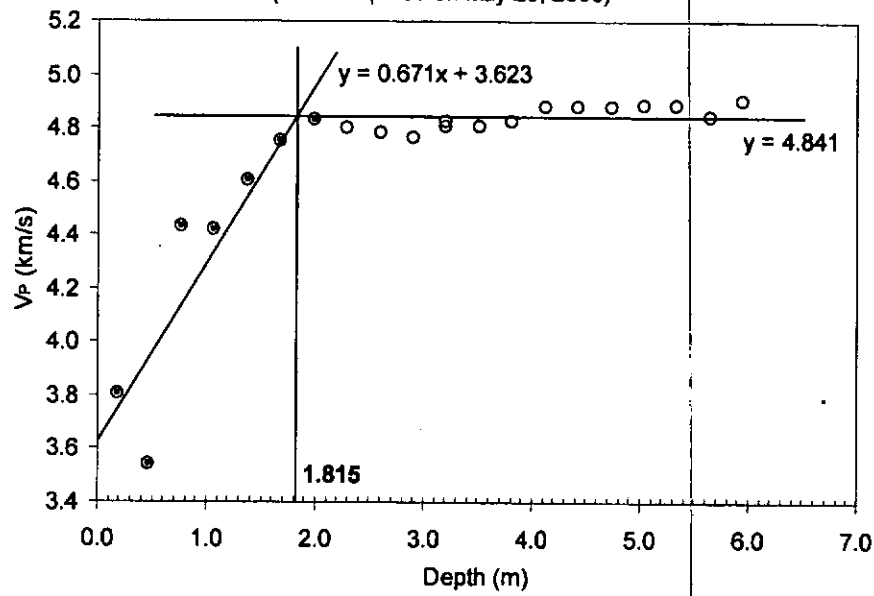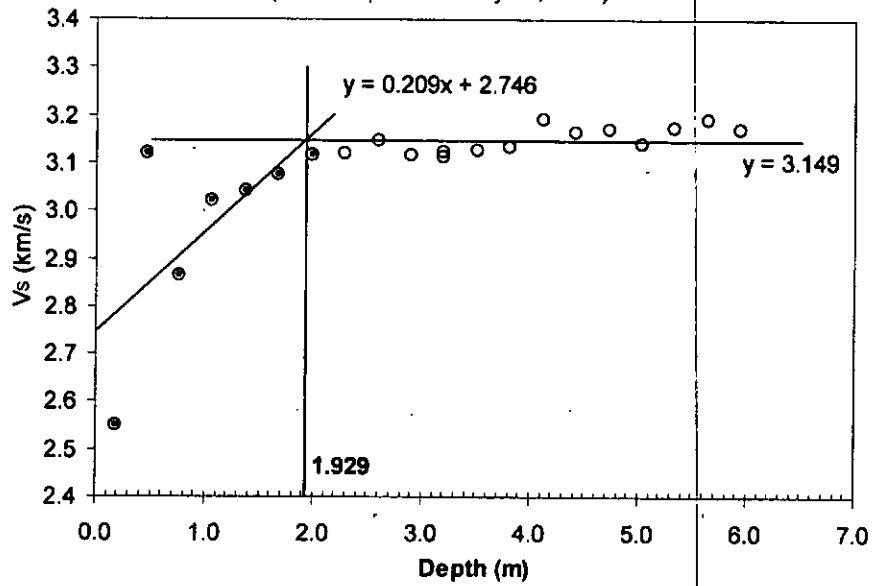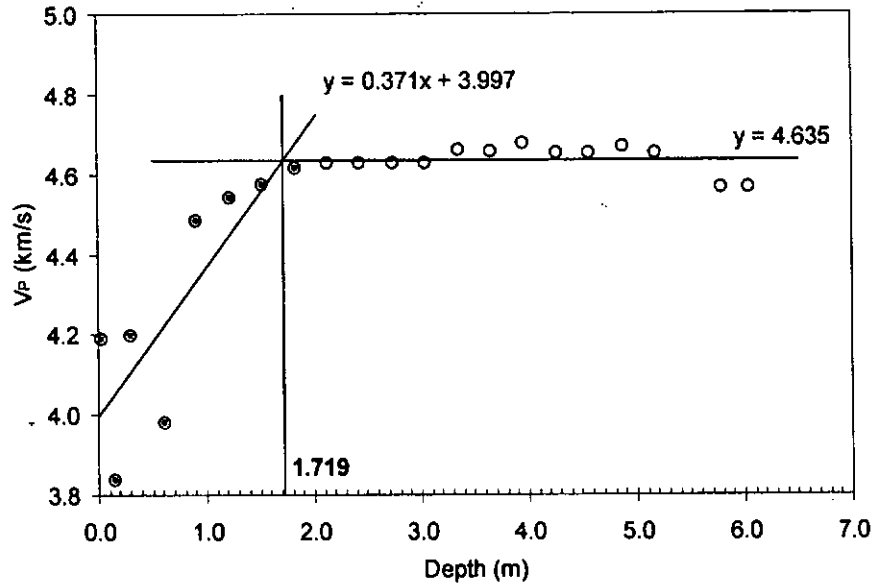
Room Q Access Drift, QGU17->QGU16, P-Wave
(Data acquired on May 25, 2000)

$y = 0.151x + 4.337$

$y = 4.488$

1.002

Room Q Access Drift, QGU17->QGU17, P-Wave
(Data acquired on May 25, 2000)

$y = 0.615x + 4.037$

$y = 4.761$

1.177

Depth (m)

V_P (km/s)

Room Q Access Drift, QGU17->QGU18, P-Wave
(Data acquired on May 25, 2000)

$y = 0.252x + 4.139$

$y = 4.502$

1.440

Depth (m)

V_P (km/s)
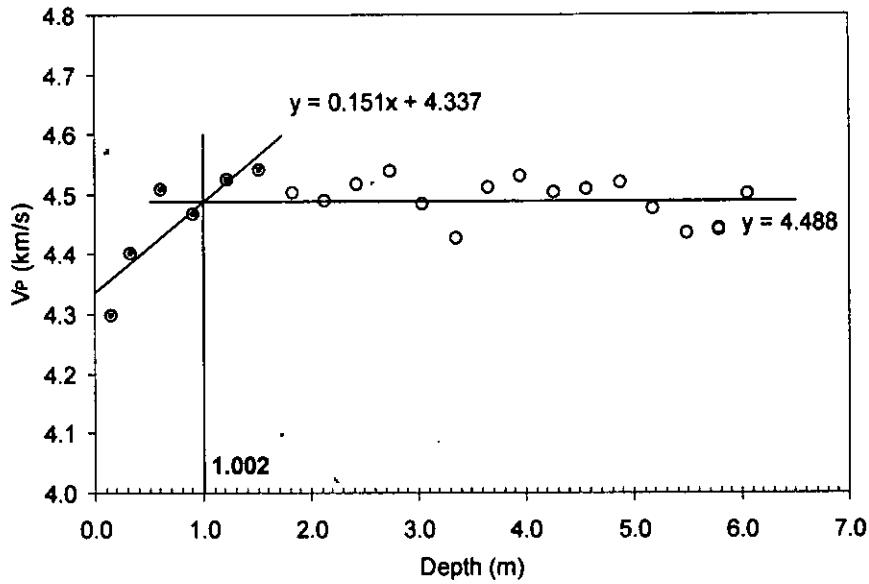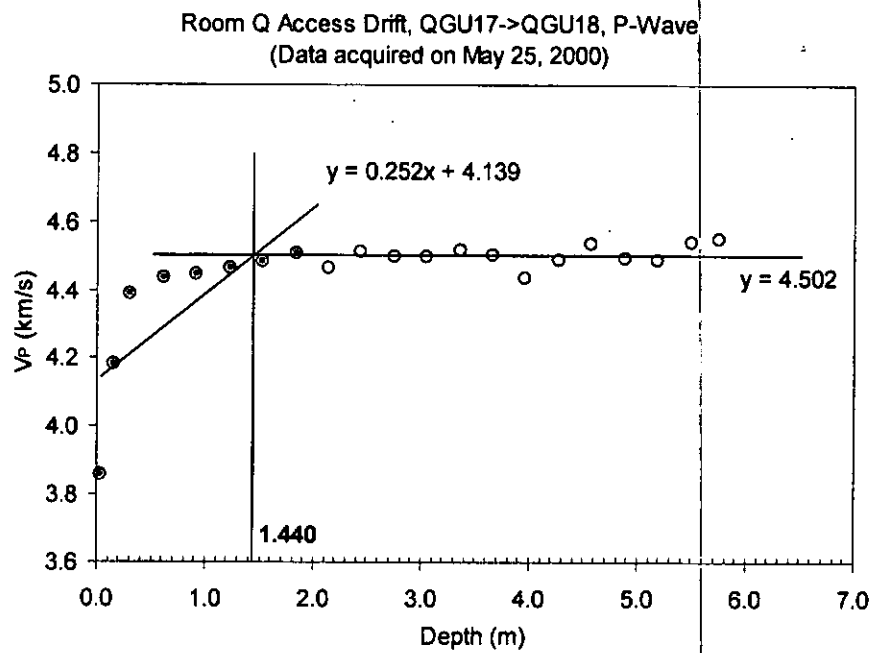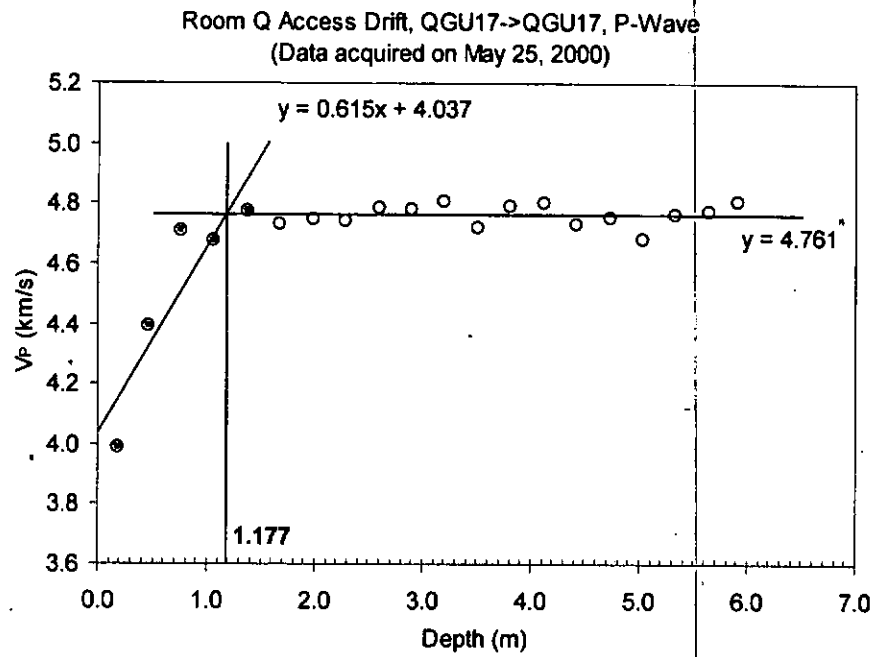
Room Q Access Drift, QGU13->QGU15, P-Wave
(Data acquired on Aug. 29, 2001)
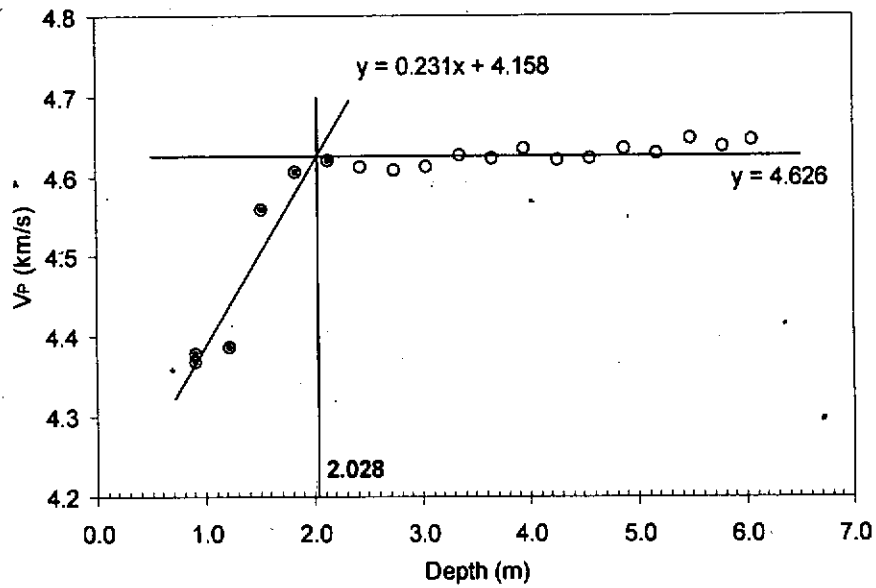
$y = 0.231x + 4.158$

$y = 4.626$

V$_P$ (km/s)

2.028

Depth (m)

Room Q Access Drift, QGU14->QGU14, P-Wave
(Data acquired on May 25, 2000)

$y = 0.966x + 2.313$

$y = 4.061$

V$_P$ (km/s)

1.809

Depth (m)

Room Q Access Drift, QGU14->QGU14, S-Wave
(Data acquired on Aug. 29, 2001)

$y = 0.798x + 1.317$

$y = 2.750$

1.796

Room Q Access Drift, QGU14->QGU15, P-Wave
(Data acquired on Aug. 28 to 29, 2001)

$y = 0.727x + 3.562$

$y = 4.573$

1.390

Room Q Access Drift, QGU14->QGU15, S-Wave
(Data acquired on Aug. 28 to 29, 2001)

$y = 0.148x + 2.341$

$y = 2.549$

1.407
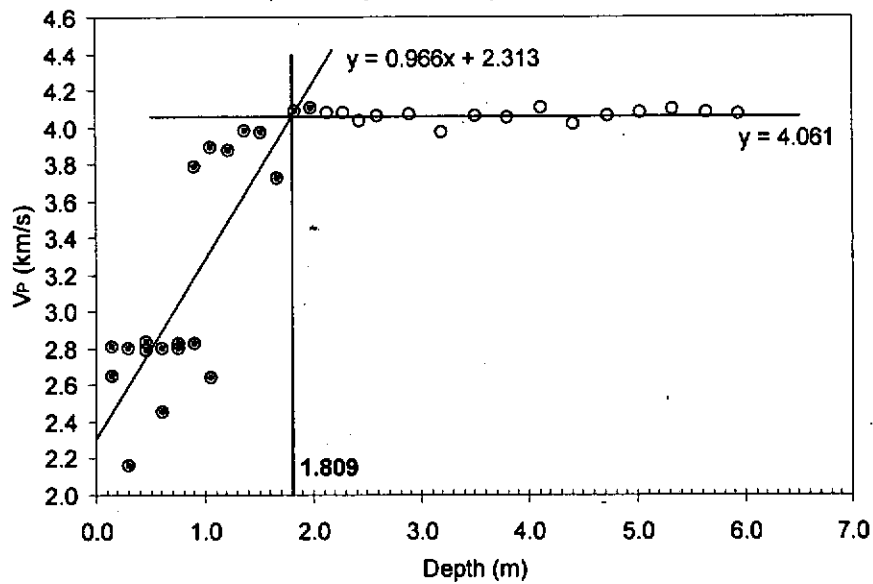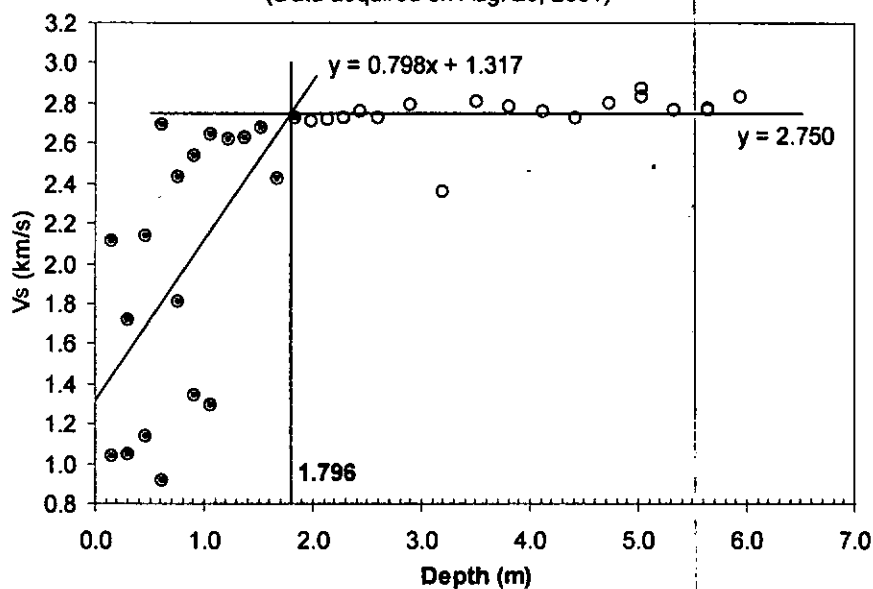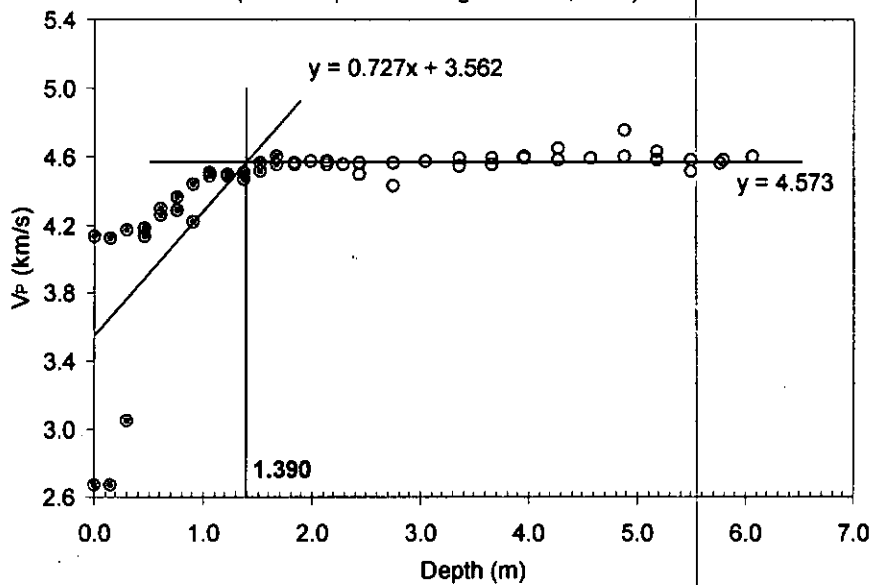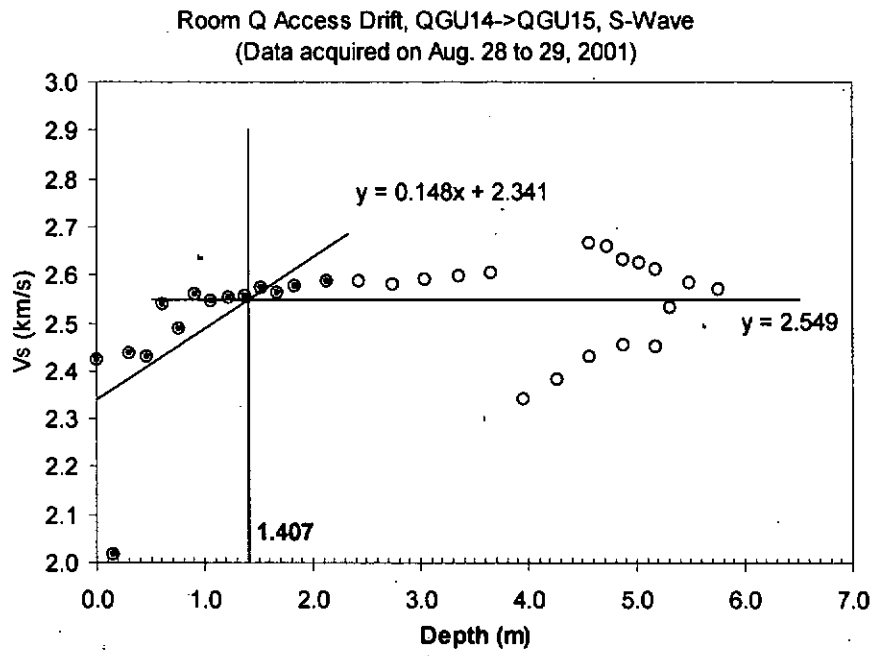
APPENDIX E: ALGEBRA AND BLOT SCRIPT FOR ILLUSTRATING THE EXTENT AND PERMEABILITY OF THE DRZ AROUND A DISPOSAL ROOM

```
===ALGEBRA================================================================
' Extent and Permeability of the DRZ around a WIPP Disposal Room
' journalized by B.Y.Park on March 6, 2007
'
ALLTIMES
'
' Mesh plots will be deformed
'
SAVE NODAL
'
' CONVERT STRESSES FROM PASCALS (Pa) TO MEGA-PASCALS (MPa)
'
SIGXX = SIGXX/1.0E+06
SIGYY = SIGYY/1.0E+06
SIGZZ = SIGZZ/1.0E+06
TAUXY = TAUXY/1.0E+06
VONMISES = VONMISES/1.0E+06
'
' Compute Sqrt(J2) and I1 (MPa)
' Compute mean pressure and limit it to 1.e-06
'
PRE = -( SIGXX + SIGYY + SIGZZ )/3.0
PRE1 = ABS(PRE) - 1.E-6
PRE2 = IFGZ(PRE1,PRE1,1.0E-6)
SJ2=VONMISES/SQRT(3.0)
I1=3.*PRE2
'
' compute damage potential in the halite
'
BLOCKS 1 3
DPOT = SJ2/I1
'
' Compute Permeability using Peach model (Pfeifle et al., 1998)
'
Ev= epsxx+epsyy+epszz    ' Volumetric strain (Chen, 1995, p.131)
Cp=2.13e-8               ' Empirical constant for damaged intact WIPP salt (m^2)
Kp1=Cp*Ev**3            ' Permeability (m^2) (Peach, 1991)
Kp=IFGZ(Kp1,Kp1,1.0e-23) ' If permeability is negative, assign Kp1=1e-23
LKp=log10(Kp)           ' Logarithm of Permeability
'
' Define time in terms of years
'
TIME = TIME/3.1536E7
'
' Delete uneeded variables
'
DELETE PRE PRE1 PRE2 SJ2 I1 Ev Cp Kp1
END
===BLOT==================================================================
det
times 0 2.74e-2 8 24 33 50 120 200 10000
zoom -2 13 -10 5
tic 1
paint dpot
ncntrs 1
crange 0 0.19
qa off
mlines
rainbow 1
plot
paint lkp
crange -20.5 -16.5
rainbow 8
copen on off
qa off
mlines
plot
exit
```

Intentionally Blank

Vugrin, Eric D ~~[signature]~~ 6/25/07

From:	Riggins, Michael
Sent:	Monday, June 25, 2007 4:00 PM
To:	Vugrin, Eric D
Cc:	Park, Byoung Yoon
Subject:	RE: signature authority

Importance: High

Eric,
I give signature authority to Eric Vugrin for all documents pertaining to the report "Analysis Report for Prediction of the Extent and Permeability of the Disturbed Rock Zone around a WIPP Disposal Room".

Mike Riggins, PhD
Sandia Nat'l Labs
Org 6711 - WIPP PA
(505) 234-0066 Carlsbad
(512) 482-0008 Austin
(505) 284-2730 Albuquerque
mriggi@sandia.gov

From: Park, Byoung Yoon
Sent: Monday, June 25, 2007 9:54 AM
To: Riggins, Michael
Subject: signature authority

Hi Dave,

I need your signature authority for our DRZ report as a technical reviewer. Could you please give me an authority?

Attached is the final version of the report.

Thanks,

Byoung-Yoon Park, Ph.D.
Sandia National Laboratories, MS1395
Perf. Assmt. & Dec. Anal. Dept., 6711
Voice: 505-234-0001
Fax: 505-234-0061
Mailing address:
4100 National Parks Highway
Carlsbad, NM 88220

Park, Byoung Yoon ~~[signature]~~ 6/25/07

From:	Holcomb, David J
Sent:	Monday, June 25, 2007 9:38 AM
To:	Park, Byoung Yoon
Subject:	RE: signature authority

The e-mail constitutes my authorization for Byoung-Yoon Park to use my signature authority for the report "Analysis Report for Prediction of the Extent and Permeability of the Disturbed Rock Zone arond a WIPP Disposal Room".

David J. Holcomb
Geomechanics
Sandia National Laboratories
PO Box 5800, MS-0751
Albuquerque, NM 87185-0751
e-mail: djholco@sandia.gov
Phone: 505-844-2157
Fax: 505-844-7354

From: Park, Byoung Yoon
Sent: Monday, June 25, 2007 8:52 AM
To: Holcomb, David J
Subject: signature authority

Hi Dave,

I need your signature authority for our DRZ report as an author. Could you please give me an authority?
Attached is the final version of the report.

Thanks,
Byoung-Yoon Park, Ph.D.
Sandia National Laboratories, MS1395
Perf. Assmt. & Dec. Anal. Dept., 6711
Voice: 505-234-0001
Fax: 505-234-0061
Mailing address:
4100 National Parks Highway
Carlsbad, NM 88220

6/25/2007